Clustered UAV Networks With Millimeter Wave Communications: A Stochastic Geometry View

Wenqiang Yi, *Student Member, IEEE*, Yuanwei Liu, *Senior Member, IEEE*, Yansha Deng, *Member, IEEE*, and Arumugam Nallanathan, *Fellow, IEEE*

***Abstract*— In order to satisfy the requirement of high throughput in most UAV applications, the potential of integrating millimeter wave (mmWave) communications with UAV networks is explored in this paper. A tractable three-dimensional (3D) spatial model is proposed for evaluating the average downlink performance of UAV networks at mmWave bands, where the locations of UAVs and users are randomly distributed with the aid of a Poisson cluster process. Moreover, an actual 3D antenna model with the uniform planar array is deployed at all UAVs to examine the impact of both azimuth and elevation angles. Based on this framework and two typical user selection schemes, closed-form approximation equations of the evaluated coverage probability and area spectral efficiency (ASE) are derived. In a noise-limited scenario, an exact expression is provided, which theoretically demonstrates that a large scale of antenna elements is able to enhance the coverage performance. Regarding the altitude of UAVs, there exists at least one optimal height for maximizing the coverage probability. Numerical results verify the proposed insight that non-line-of-sight transmission caused by obstacles have negligible effects on the proposed system. Another interesting result is that the ASE can be maximized by optimizing both the targeted data rate and the density of UAVs.**

***Index Terms*— Millimeter wave, Poisson cluster process, stochastic geometry, unmanned aerial vehicle.**

I. Introduction

THANKS to the low cost and high mobility, unmanned aerial vehicle (UAV) networks have kindled the strong attention of academia recently [2]. In contrast to conventional terrestrial base stations (BSs), the maneuverability of UAVs creates various new approaches for enhancing the coverage and capacity of wireless networks. Concerning the coverage enhancing ability, UAVs are capable of offering temporary connections to uncovered devices efficiently. This situation is frequently caused by damaged BSs, severe shadowing, and so forth [3]. Therefore, UAV networks have enormous potential in several special applications [4], [5], such as reconnaissance, firefighting, disaster rescue, etc. Regarding the capacity enhancing ability, the height and position of UAVs can be adjusted to provide a robust channel condition which contributes to high system throughput, especially in hot spot regions [6]. Accordingly, numerous research efforts have been made to design the controlling strategies of UAVs [6]–[9]. Considering the controllable moving trajectory of UAVs, the completion time and the energy consumption was evaluated in [6] and [7], respectively. Based on users' behaviors, the locations and content cached at UAVs are optimized in [8] to maximize the quality-of-experience (QoE). After that, the joint optimization of spectrum allocation, user association, and content distribution in UAV systems is studied in [9].

Benefited by these abilities, UAV networks are frequently designed for transmitting control commands and large data packages (e.g., videos) to users [5]. Therefore, most UAV systems require fast responses and high data rate links. To this end, millimeter wave (mmWave) with massive available bandwidth resources becomes an ideal carrier frequency candidate. In contrast to the traditional cellular networks with sub-6 GHz, mmWave has two distinctive features [10]. The first property is the small wavelength, which helps to shorten the physical size of antenna elements, thereby enlarging the antenna arrays at all transceivers [11], [12]. With the aid of large antennas, it is possible to implement sharp directional beamforming in mmWave equipment for enhancing the desired signals and weakening interference [13]. The second property is the sensitivity to blockages. Due to this property, mmWave signals transmitted via non-line-of-sight (NLOS) links experience more severe path loss than those through line-of-sight (LOS) links [13]–[15]. A large number of articles have investigated the above-mentioned features [10], [16], [17]. An actual antenna array pattern, namely uniform linear array (ULA), was presented in [16], which analyzed the effect of azimuth angles. Regarding the blockage environment, a two-dimensional (2D) stochastic blockage model was introduced to separate LOS and NLOS transmission [10]. Considering the height of transceivers, a three-dimensional (3D) urban scenario was analyzed in [17], which propounded a tractable transmission model.

A. Motivation and Related Works

As aforementioned, we conclude that there exist two main benefits for deploying mmWave communications to UAV networks. One is that the large available spectrum of

Manuscript received June 6, 2019; revised October 5, 2019, January 9, 2020, and March 6, 2020; accepted March 6, 2020. Date of publication March 13, 2020; date of current version July 15, 2020. This work was supported by the U.K. Engineering and Physical Sciences Research Council (EPSRC) under Grant EP/N029720/2. This article was presented in part at the IEEE International Conference on Communications (ICC) Workshops, China, May 2019 [1]. The associate editor coordinating the review of this article and approving it for publication was D. B. Da Costa. *(Corresponding author: Yuanwei Liu.)*

Wenqiang Yi, Yuanwei Liu, and Arumugam Nallanathan are with the School of Electronic Engineering and Computer Science, Queen Mary University of London, London E1 4NS, U.K. (e-mail: w.yi@qmul.ac.uk; yuanwei.liu@qmul.ac.uk; a.nallanathan@qmul.ac.uk).

Yansha Deng is with the Department of Informatics, King's College London, London WC2B 4BG, U.K. (e-mail: yansha.deng@kcl.ac.uk).

Color versions of one or more of the figures in this article are available online at http://ieeexplore.ieee.org.

Digital Object Identifier 10.1109/TCOMM.2020.2980787

mmWave is able to substantially boost the capacity of UAV networks and hence satisfying the requirement of prompt responses [18]–[21]. The other advantage is that the data traffic of UAV networks can be significantly enlarged by using mmWave since mmWave communications are capable of offering high throughput in short-range transmission [22]. In most applications, UAVs are able to provide obstacle-free short-range communications by adjusting their locations and altitudes.

Motivated by these potential advantages, we are interested in the average performance of mmWave-enabled UAV networks. Note that stochastic geometry is an efficient mathematical approach for capturing the average behavior of networks [23]–[25]. Recent articles [26]–[29] have utilized this theoretical tool to design various spatial models for UAV networks with sub-6 GHz. The authors in [26] modeled the locations of UAVs as a uniform binomial point process (BPP). Based on this wireless system, the correlation between the coverage probability and the height of UAVs was analyzed. Since the BPP is a finite case of Poisson point processes (PPPs), to enhance the generality, the served users were located according to a PPP in [27] to estimate the outage performance in non-orthogonal multiple access (NOMA)-aided UAV systems. Considering the randomness of BSs, this framework was extended to a more general case that UAVs and BSs were modeled as two independent PPPs [28]. The authors in [29] have relaxed the fixed height assumption in previous papers by considering a sphere region to generate a 3D PPP framework. Regarding mmWave networks, stochastic geometry has also been widely applied. Initial papers focused on the PPP scheme [10], [30], [31] ignoring clustered distribution scenarios. For the small cells with clustered devices, the authors in [22], [32] studied another promising framework modeled by Poisson Cluster Process (PCP). This framework is also suitable for characterizing short-range mmWave networks.

Although several research efforts have fostered UAV and mmWave networks, to the best of our knowledge, the system design of mmWave-enabled clustered UAV networks is still at the early stage. We strive to explore the performance of such systems, especially evaluating key metrics, e.g., the coverage probability and area spectral efficiency (ASE). More particularly, we attempt to answer three main questions as follows:

- **Question 1:** Does the high altitude of UAVs enhance the coverage performance when comparing with conventional terrestrial networks?
- **Question 2:** How do the adjustable parameters of the considered mmWave-enabled UAV system affect average ASE?
- **Question 3:** Are the considered mmWave-enabled UAV networks noise-limited or interference-limited?

B. Contributions

In this article, we introduce a promising 3D spatial model for clustered UAV networks with mmWave communications. Considering the clustered property, we employ the PCP scheme to model the location of UAVs and users. Based on this framework, we provide two user selection schemes for estimating the system performance. The main contributions of our article can be summarized as:

- We propose a new framework for analyzing the coverage performance and ASE of mmWave-enabled UAV networks. In this framework, we consider an actual 3D antenna array pattern, namely uniform planar array (UPA), to evaluate the effect of both azimuth and elevation angles. Moreover, we derived a closed-form expression for the phase shifted antenna gain.
- We introduce two different user selection schemes: 1) *Random Selection (RS) Scheme*, where the serving UAV randomly choose one of intra-cluster users as the receiver; and 2) i*-th Nearest (IN) Scheme*, where the served user is the i-th closest node to the intra-cluster serving UAV. Based on these schemes, we characterize the distribution of both intra-cluster communication distances and inter-cluster interfering distances.
- We introduce Laplace transform of interference for tractability of the analysis. Tight closed-form approximation expressions for coverage probabilities and ASE under two schemes are deduced based on the proposed distance distributions. With a noise-limited assumption, we figure out an exact closed-form expression for the coverage probability. It analytically demonstrates that large antenna scale benefits the coverage performance in our system.
- We demonstrate that: 1) an optimal altitude of UAVs exists for maximizing coverage probabilities; 2) in order to increase ASE, both the density of UAVs and the targeted rate can be optimized; 3) the impact of NLOS transmission is negligible, especially when the density of obstacles is small; 4) with the increase of the UAV density, our system gradually changes from a noise-limited status into an interference-limited status; and 5) compared with 28 GHz, higher carrier frequencies are able to compensate for the more severe path loss by employing more antenna elements.

C. Organization and Notations

This work is presented as follows: In Section II, we describe our network model. In Section III, the distribution of the distance between the typical UAV and the corresponding user is discussed. In Section IV, we deduce theoretical equations for coverage probabilities and ASE. In Section V, Monte Carlo (MC) simulations and numerical results are illustrated. In Section VI, we propose the conclusion and the future work. Notations in this paper are listed in Table I.

II. Network Model

A. Spatial Distribution

In this paper, we consider the downlink of clustered UAV networks with mmWave communications. The spatial model is shown in Fig. 1. It follows a typical variant of Thomas cluster process [22], [33], where *parent points* representing cluster centers are modeled as a homogeneous PPP Φ with density λ. Around each parent point, the corresponding *daughter points* are independently and identically distributed (i.i.d.) according to symmetric normal distributions with a variance σ^2. For one

TABLE I
TABLE OF NOTATIONS

Notation	Description
Φ; λ	PPP modeled location of UAVs; density of UAVs
$\mathbb{U}_{\mathbf{p}}$; σ; N;	Normal distributed locations of users; standard deviation; the number of users in each cluster
h_u; h_v; $\hat{h}$	Height of users; height of UAVs; height difference $\hat{h} = h_v - h_u$
λ_a; λ_b; ϵ	Ratio of the building area to the total area; density of buildings; scale parameter of the building distribution
$\mathbb{Z}^*$; δ_r	Set of all natural numbers; discrete horizontal communication distances in terms of the continuous distance r
N_κ; C_κ; α_κ	Nakagami parameter; intercept; path loss exponent ($\kappa \in \{L, N\}$)
M_x; M_y; M	Number of antenna elements in the x-axis direction; that in the y-axis direction; antenna scale $M = M_x \times M_y$
$h_{\mathbf{v}}$;P	Small-scale parameter; transmit power of UAVs
$\phi_{\mathbf{v}}$; $\theta_{\mathbf{v}}$	Azimuth angles; elevation angles for the channel vector
d_x; d_y; λ_w	Antenna spacing in the x-axis direction; that in the y-axis direction; wavelength of the carrier
$\psi_{\mathbf{v}}$; $\vartheta_{\mathbf{v}}$	Azimuth angles; elevation angles for the optimal analog beamforming vector
n_0; σ_n^2	Thermal noise; relative noise power
$\mathbb{B}(.)$; $\mathbb{P}[.]$; ${}_2F_1(.)$	Bernoulli random variable; probability function; Gauss hypergeometric function
$\otimes$; H; tr(.)	Kronecker product; symbol for conjugate transpose; trace of matrixes

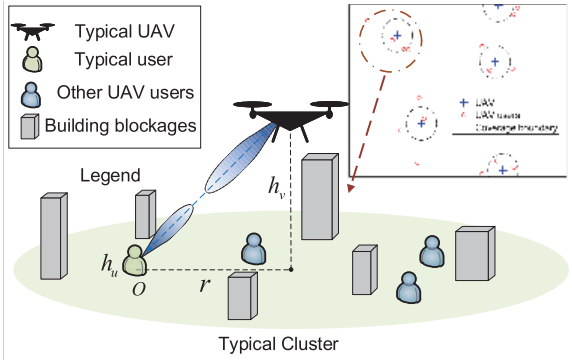

Fig. 1. The layout of downlink UAV networks with mmWave communications. The clustered users are distributed as a typical variant of Thomas cluster process with a height of h_u and the central UAVs have a height of h_v.

parent point at $\mathbf{p} \in \Phi(\mathbf{p} \in \mathbb{R}^2)$, its daughter points are denoted by $\mathbb{U}_{\mathbf{p}}$ and the number of these points is $|\mathbb{U}_{\mathbf{p}}| = N$. As a consequence, the density function of the distance from a daughter point at $\mathbf{d} \in \mathbb{U}_{\mathbf{p}}(\mathbf{d} \in \mathbb{R}^2)$ to its parent point at $\mathbf{p}$ is as follows:

$$f_D(\mathbf{d}) = \frac{1}{2\pi\sigma^2} \exp\left(-\frac{\|\mathbf{d}-\mathbf{p}\|^2}{2\sigma^2}\right). \quad (1)$$

Note that realistic users with similar purposes are frequently gathered together to form a cluster. By introducing the altitude of users h_u in our system, the location of clustered users can be represented by $\mathbf{u} = (\mathbf{d}, h_u)$ and $\mathbf{u} \in \mathbb{R}^3$. Regarding UAVs, we assume each rotary-wing UAV hovers above one cluster center at a height h_v to provide a fair service to the entire intra-cluster users.[1] As a result, the location of each UAV can be denoted by $\mathbf{v} = (\mathbf{p}, h_v)$ and $\mathbf{v} \in \mathbb{R}^3$.

Without loss of generality, we randomly choose one user to be a *typical user*, which is fixed at $\mathbf{u}_0 = (0, 0, h_u)$. The corresponding serving UAV and cluster are regarded as a *typical UAV* and a *typical cluster*, respectively. Two different user selection schemes are introduced in this article: 1) RS scheme, where the typical user is chosen randomly; and 2) IN scheme, where the typical user is the i-th closest intra-cluster node to the typical UAV.

[1]Since the movement of UAVs is slow when serving users, the Doppler shift has limited impact on our system. Practical measurements [34] have demonstrated that in mmWave communications, the angular spread of each path is small. High directional beamforming is able to further reduce the multi-path caused angular spread [35]. Therefore, this paper ignores Doppler effects.

B. Blockage Model

To evaluate the average impact of obstacles, we utilize a typical 3D blockage model based on a stochastic process [17]. This blockage model defines the urban environment, where the density of buildings (obstacles), the ratio of the building area to the total area, and the scale parameter of the Rayleigh distributed building heights are λ_b m^{-2}, λ_a, and ϵ, respectively. After applying this model, the probability of transmission no being blocked can be calculated with the aid of the corresponding horizontal communication distance r, which is given by [28]

$$p_L(\delta_r) = \prod_{n=0}^{\max(0,\delta_r-1)} \left(1 - \exp\left(-\left(\frac{\delta_r h_v - (n+1/2)\hat{h}}{\sqrt{2}\epsilon\delta_r}\right)^2\right)\right), \quad (2)$$

where $\hat{h} = h_v - h_u$, $\delta_r = \lfloor r\sqrt{\lambda_a\lambda_b} \rfloor$ and the subscript r represents the independent variable of δ_r. The UAV-ground elevation angle is omitted in (2) as this angle is decided by two parameters ($\hat{h}$ and r) which have been considered in (2). It is straightforward that the probability for NLOS transmission is $p_N(\delta_r) = 1 - p_L(\delta_r)$.

Remark 1: Based on the definition of δ_r, the continuous variable r can be divided into multiple steps. For example, the step $\delta_r = S_t$ represents the distance range $\left(\frac{S_t}{\sqrt{\lambda_a\lambda_b}} \leq r < \frac{S_t+1}{\sqrt{\lambda_a\lambda_b}}\right)$. It is worth noting that for each step, $p_L(\delta_r)$ has the same value. Therefore, we define that δ_r is the discrete horizontal communication distance.

When considering a practical close-in (CI) free-space path loss model [36] and the LOS/NLOS conditions as mentioned in (2), the path loss function of our UAV networks is as follows:

$$\mathrm{L}(r) = \sum_{\kappa\in\{L,N\}} \mathbb{B}\left(p_\kappa(\delta_r)\right) C_\kappa \left(r^2 + \hat{h}^2\right)^{-\frac{\alpha_\kappa}{2}}, \quad (3)$$

where C_κ denotes the intercept and α_κ is the path loss exponent. These two parameters are statistically derived from practical measurements. The $\kappa = L$ and $\kappa = N$ represent LOS and NLOS links, respectively. $\mathbb{B}(t)$ is a Bernoulli random variable with a probability of success t.

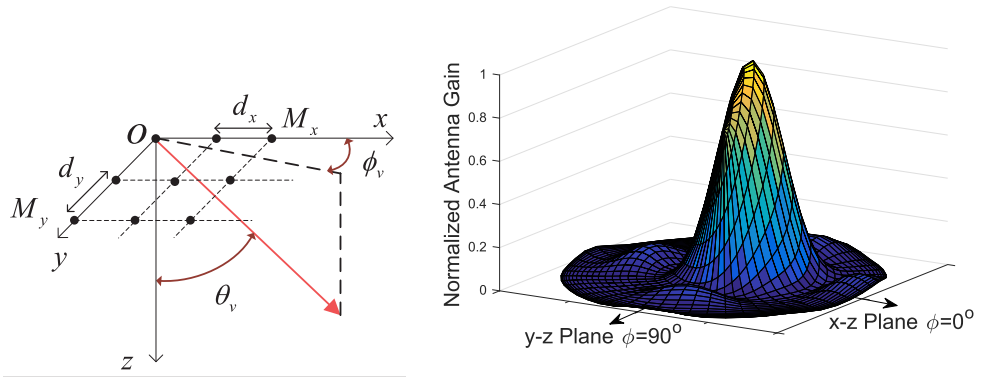

(a) The deployment of antenna elements in uniform planar array pattern.

(b) Normalized antenna gain with $\psi_{\mathbf{v}} = \frac{\pi}{4}$, $\vartheta_{\mathbf{v}} = \frac{\pi}{18}$, $2d_x = 2d_y = \lambda_w = \frac{3\times10^8\ m/s}{28\ GHz}$, and $M_x = M_y = 4$.

Fig. 2. Illustration of the considered antenna pattern with uniform planar array.

C. Uniform Planar Array

Due to the limited carrying ability of users, the antenna scale at the user side is smaller than that at the UAV side. In this paper, we focus on the analyzing of UAVs' antenna effects, which forming a multiple-input single-output (MISO) system [30]. Note that MISO systems ignore the antenna beamforming at the user side, which overestimates the interference. Therefore, the considered MISO model can be regarded as the lower bound of multiple-input-multiple-output (MIMO) systems. A typical 3D antenna pattern [37], [38] named UPA is deployed at all UAVs. Each UAV antenna is composed of $M = M_x \times M_y$ elements as illustrated in Fig. 2(a). The d_x is the antenna spacing in the x-axis direction and d_y is that in the y-axis direction. The λ_w is the wavelength of carriers. Regarding served users, a single-antenna pattern is considered. For a transmission channel from a transmitting UAV at $\mathbf{v}$ to the typical user, the corresponding azimuth and elevation angles are respectively denoted by $\phi_{\mathbf{v}}$ and $\theta_{\mathbf{v}}$, which obeys $\phi_{\mathbf{v}} \in (-\pi, \pi]$ and $\theta_{\mathbf{v}} \in (-\frac{\pi}{2}, \frac{\pi}{2}]$. The channel vector can be expressed as [10], [30]

$$\boldsymbol{h}_{\mathbf{v}} = \sqrt{M} h_{\mathbf{v}} \boldsymbol{a}\left(\phi_{\mathbf{v}}, \theta_{\mathbf{v}}\right), \tag{4}$$

where $h_{\mathbf{v}}$ represents a parameter for small-scale Nakagami fading channels. The $\boldsymbol{a}\left(\phi_{\mathbf{v}}, \theta_{\mathbf{v}}\right)$ is the transmit array response vector, which is the multiplication of one array response vector along the x-axis $\boldsymbol{a}_x\left(\phi_{\mathbf{v}}, \theta_{\mathbf{v}}\right)$ and one array response vector along the y-axis $\boldsymbol{a}_y\left(\phi_{\mathbf{v}}, \theta_{\mathbf{v}}\right)$ [37], [38]:

$$\boldsymbol{a}\left(\phi_{\mathbf{v}}, \theta_{\mathbf{v}}\right) = \boldsymbol{a}_x\left(\phi_{\mathbf{v}}, \theta_{\mathbf{v}}\right) \otimes \boldsymbol{a}_y\left(\phi_{\mathbf{v}}, \theta_{\mathbf{v}}\right), \tag{5}$$

where

$$\boldsymbol{a}_x\left(\phi_{\mathbf{v}}, \theta_{\mathbf{v}}\right) = \frac{1}{\sqrt{M_x}} \times \Big[1, \ldots, e^{j\frac{2\pi d_x}{\lambda_w} m_x \sin\theta_{\mathbf{v}} \cos\phi_{\mathbf{v}}}, \ldots, e^{j\frac{2\pi d_x}{\lambda_w}(M_x-1)\sin\theta_{\mathbf{v}}\cos\phi_{\mathbf{v}}}\Big]^T, \tag{6}$$

$$\boldsymbol{a}_y\left(\phi_{\mathbf{v}}, \theta_{\mathbf{v}}\right) = \frac{1}{\sqrt{M_y}} \times \Big[1, \ldots, e^{j\frac{2\pi d_y}{\lambda_w} m_y \sin\theta_{\mathbf{v}} \sin\phi_{\mathbf{v}}}, \ldots, e^{j\frac{2\pi d_y}{\lambda_w}(M_y-1)\sin\theta_{\mathbf{v}}\sin\phi_{\mathbf{v}}}\Big] \tag{7}$$

and $\otimes$ is the Kronecker product. The m_x and m_y are integers within $[0, M_x - 1]$ and $[0, M_y - 1]$, respectively.

D. Antenna Beamforming

In order to achieve a low-cost time-space processing technique, we employ an analog beamforming pattern, where phase shifters are employed to control the beam direction. More particularly, if the azimuth and elevation angles of departure (AoD) from the UAV at $\mathbf{v}$ to its served user are $\psi_{\mathbf{v}}$ and $\vartheta_{\mathbf{v}}$, respectively, the optimal analog beamforming is obtained by aligning the direction of the beam with AoDs $\psi_{\mathbf{v}}$ and $\vartheta_{\mathbf{v}}$. Therefore, the optimal analog beamforming vector is given by

$$\boldsymbol{w}_{\mathbf{v}} = \boldsymbol{w}_{\text{opt}} = \boldsymbol{a}\left(\psi_{\mathbf{v}}, \vartheta_{\mathbf{v}}\right). \tag{8}$$

The typical UAV at $\mathbf{v}_0 = (\mathbf{p}_0, h_v)$ adjusts its antenna beam towards the typical user for achieving optimal analog beamforming, namely $\phi_{\mathbf{v}_0} = \psi_{\mathbf{v}_0}$ and $\theta_{\mathbf{v}_0} = \vartheta_{\mathbf{v}_0}$. We assume that the transmit power at all UAVs is a constant P. As a result, the received signal at the typical user with the interfering UAV at $\mathbf{v} = (\mathbf{p}, h_v)$ is given by

$$y_s = \underbrace{\sqrt{P\mathrm{L}\left(\|\mathbf{p}_0\|\right)} \boldsymbol{h}_{\mathbf{v}_0}^{\mathrm{H}} \boldsymbol{w}_{\mathbf{v}_0} s_{\mathbf{v}_0}}_{\textbf{Desired Signal}} + \underbrace{\sum_{\mathbf{p}\in\Phi\setminus\mathbf{p}_0} \sqrt{P\mathrm{L}\left(\|\mathbf{p}\|\right)} \boldsymbol{h}_{\mathbf{v}}^{\mathrm{H}} \boldsymbol{w}_{\mathbf{v}} s_{\mathbf{v}}}_{\textbf{Interference}} + \underbrace{n_0}_{\textbf{Noise}}, \tag{9}$$

where the superscript H is conjugate transpose. n_0 represents thermal noise.

Based on this MISO system, the effective product of antenna beamforming gain and fading channel gain for one UAV at $\mathbf{v}$ is shown as follows [30], [39]:

$$\begin{aligned} H_{\mathbf{v}} &\triangleq \left|\mathrm{tr}(\boldsymbol{h}_{\mathbf{v}}^{\mathrm{H}} \boldsymbol{w}_{\mathbf{v}})\right|^2 = M|h_{\mathbf{v}}|^2 \left|\mathrm{tr}(\boldsymbol{a}^{\mathrm{H}}\left(\phi_{\mathbf{v}}, \theta_{\mathrm{v}}\right) \boldsymbol{a}\left(\psi_{\mathbf{v}}, \vartheta_{\mathbf{v}}\right))\right|^2 \\ &= M|h_{\mathbf{v}}|^2 \mathcal{G}\left(\phi_{\mathbf{v}}, \theta_{\mathbf{v}}, \psi_{\mathbf{v}}, \vartheta_{\mathbf{v}}\right), \end{aligned} \tag{10}$$

where $\mathrm{tr}(A)$ denotes the trace of the matrix A. As we adopt Nakagami small fading channel with the parameter N_κ in this work, $|h_{\mathbf{v}}|^2$ is a Gamma random variable and N_κ is assumed to be a positive integer for simplicity [10]. The antenna gain function is represented by $\mathcal{G}(.)$, which is illustrated in Fig. 2(b).

Since the typical UAV adjusts its directional beam towards the typical user as mentioned earlier, $\mathcal{G}\left(\phi_{\mathbf{v}_0}, \theta_{\mathbf{v}_0}, \psi_{\mathbf{v}_0}, \vartheta_{\mathbf{v}_0}\right) \triangleq 1$. Regarding an interfering UAV at $\mathbf{v}$, the antenna gain function for such UAV is at the bottom of this page.

To simplify the analysis, we assume that $\vartheta_{\mathbf{v}} = 0$, which means the UPA faces to its served user. Regarding the rest angles, $\psi_{\mathbf{v}}$ and $\phi_{\mathbf{v}}$ are uniformly distributed over $[-\pi, \pi]$. The $\sin\theta_{\mathbf{v}} = \omega$ is uniformly distributed over $[-1, 1]$ [40]. Therefore, (11) can be rewritten as follows:

$$\begin{aligned}\mathcal{G}&\left(\phi_{\mathbf{v}}, \theta_{\mathbf{v}}, \psi_{\mathbf{v}}, \vartheta_{\mathbf{v}}\right)\\ &= \mathcal{G}\left(\phi_{\mathbf{v}}, \omega\right)\\ &= \frac{\sin^2\left(M_x \frac{\pi d_x}{\lambda_w}\omega\cos\phi_{\mathbf{v}}\right)\sin^2\left(M_y \frac{\pi d_y}{\lambda_w}\omega\sin\phi_{\mathbf{v}}\right)}{M^2\sin^2\left(\frac{\pi d_x}{\lambda_w}\omega\cos\phi_{\mathbf{v}}\right)\sin^2\left(\frac{\pi d_y}{\lambda_w}\omega\sin\phi_{\mathbf{v}}\right)}. \quad (12)\end{aligned}$$

In this paper, we consider a square UPA that $d_x = d_y$ and $M_x = M_y$. With the aid of (12), we find that the antenna gain obeys $\mathcal{G}(\phi_{\mathbf{v}}) = \mathcal{G}(\phi_{\mathbf{v}} + \frac{n\pi}{2})|_{n=0,1,2,\ldots}$, which means $\mathcal{G}(\phi_{\mathbf{v}})$ has a period of $\frac{\pi}{2}$. Moreover, since $\mathcal{G}(\phi_{\mathbf{v}})$ is an even function, the values in the range $[-\frac{\pi}{4}, 0]$ correspond to those in $[0, \frac{\pi}{4}]$. Note that $\mathcal{G}(0) \leq \mathcal{G}(\phi_{\mathbf{v}}) \leq \mathcal{G}(\frac{\pi}{4})$ since $\mathcal{G}(\phi_{\mathbf{v}})$ is a monotonic increasing function when $\phi_{\mathbf{v}} \in [0, \frac{\pi}{4}]$. For arbitrary A, $\mathbb{E}\left[\exp(-A\mathcal{G}(\phi_{\mathbf{v}}, \omega))\right]$ equals to $(\exp(-A\mathcal{G}(\phi_c, \omega)))$, where $\phi_c \in [0, \frac{\pi}{4}]$ is constant. Therefore, we provide a simplified antenna model with $\phi_{\mathbf{v}} \equiv \phi_c$. The comparison between the actual and simplified antenna model is shown in Fig. 3. This simplified antenna pattern has a negligible difference with the actual one, especially for the regions that $\mathcal{G}(.) \geq \frac{1}{2}$. Based on this assumption, the complex antenna gain in (12) can be rewritten as:

$$\begin{aligned}\mathcal{G}(\omega) &= \mathcal{G}(\phi_c, \omega)\\ &= \frac{\sin^2\left(M_x \frac{\pi d_x}{\lambda_w}\omega\cos\phi_c\right)\sin^2\left(M_y \frac{\pi d_y}{\lambda_w}\omega\sin\phi_c\right)}{M^2\sin^2\left(\frac{\pi d_x}{\lambda_w}\omega\cos\phi_c\right)\sin^2\left(\frac{\pi d_y}{\lambda_w}\omega\sin\phi_c\right)}. \quad (13)\end{aligned}$$

In (13), there is only one variable left. This simplification enhances the evaluation efficiency.

E. Signal Model

Since the onboard energy in UAV systems is limited [7], we assume that UAVs are constantly transmitting information during the entire serving period. Therefore, all UAVs are regarded as active in our system. In addition to the typical UAV, remaining UAVs offer interference. Based on aforementioned assumptions, the signal-to-interference-plus-noise-ratio (SINR) equation in the proposed clustered UAV networks can be expressed as

$$\begin{aligned}\Upsilon\left(\|\mathbf{p}_0\|\right) &= \frac{P\mathrm{L}\left(\|\mathbf{p}_0\|\right)H_{\mathbf{v}_0}}{P\sum\limits_{\mathbf{p}\in\Phi\setminus\mathbf{p}_0}\mathrm{L}\left(\|\mathbf{p}\|\right)H_{\mathbf{v}} + |n_0|^2}\\ &= \frac{\mathrm{L}\left(\|\mathbf{p}_0\|\right)|h_{\mathbf{v}_0}|^2}{\sum\limits_{\mathbf{p}\in\Phi\setminus\mathbf{p}_0}\mathrm{L}\left(\|\mathbf{p}\|\right)|h_{\mathbf{v}}|^2\mathcal{G}\left(\phi_{\mathbf{v}}, \omega\right) + \sigma_n^2}, \quad (14)\end{aligned}$$

where $\sigma_n^2 = \frac{|n_0|^2}{PM}$ is the relative noise power regarding to the transmit power P and the antenna scale M.

III. Distribution of Distance

We define two different horizontal communication distances as follows: 1) the *typical distance*, which is the horizontal distance between the typical user and the typical UAV; and 2) the *interfering distances*, which are the horizontal distances between the typical user and interfering UAVs. In this section, we analyze the distribution of these distances. Before that, we primarily present the PDF and the cumulative distribution function (CDF) of *Rayleigh distributions* to simplify notations. The PDF of Rayleigh distributions is

$$f_p(x, \sigma) = \frac{x}{\sigma^2}\exp\left(-\frac{x^2}{2\sigma^2}\right), \quad (x \geq 0), \quad (15)$$

where σ is the standard deviation as shown in (1). Additionally, the CDF of Rayleigh distributions is given by

$$F_c(x, \sigma) = 1 - \exp\left(-\frac{x^2}{2\sigma^2}\right), \quad (x \geq 0). \quad (16)$$

A. Distance Distributions in Random Selection Scheme

In this part, we first analyze the distribution of the typical distance and then the distribution of the interfering distances.

1) Distribution of Typical Distance: Assuming all horizontal distances between intra-cluster users and the typical UAV are denoted by a set $\{U_i\}_{i=1:N}$. We define $u_i = \|\mathbf{p}_0 - \mathbf{d}_i\|$ $(\mathbf{d}_i \in \mathbb{U}_{\mathbf{p}_0})$ is the realization of U_i and $u_1 \leq \ldots \leq u_k \leq \ldots u_N$, namely u_i is the horizontal distance from the i-th closest intra-cluster user to the typical UAV.

In the RS scheme, the typical user is randomly selected from the typical cluster. Noted that users are i.i.d. such that the subscript i can be dropped from U_i and u_i. As a consequence, the PDF of u is given by [22], [33]

$$f_{RS}(u) = f_p(u, \sigma). \quad (17)$$

$$\begin{aligned}\mathcal{G}\left(\phi_{\mathbf{v}}, \theta_{\mathbf{v}}, \psi_{\mathbf{v}}, \vartheta_{\mathbf{v}}\right) &= \frac{1}{M^2}\left|\sum_{m=1}^{M_x} e^{j(m-1)\frac{2\pi d_x}{\lambda_w}(\sin\vartheta_{\mathbf{v}}\cos\psi_{\mathbf{v}} - \sin\theta_{\mathbf{v}}\cos\phi_{\mathbf{v}})}\sum_{n=1}^{M_y} e^{j(n-1)\frac{2\pi d_y}{\lambda_w}(\sin\vartheta_{\mathbf{v}}\sin\psi_{\mathbf{v}} - \sin\theta_{\mathbf{v}}\sin\phi_{\mathbf{v}})}\right|^2\\ &= \frac{\sin^2\left(M_x \frac{\pi d_x}{\lambda_w}(\sin\vartheta_{\mathbf{v}}\cos\psi_{\mathbf{v}} - \sin\theta_{\mathbf{v}}\cos\phi_{\mathbf{v}})\right)\sin^2\left(M_y \frac{\pi d_y}{\lambda_w}(\sin\vartheta_{\mathbf{v}}\sin\psi_{\mathbf{v}} - \sin\theta_{\mathbf{v}}\sin\phi_{\mathbf{v}})\right)}{M^2\sin^2\left(\frac{\pi d_x}{\lambda_w}(\sin\vartheta_{\mathbf{v}}\cos\psi_{\mathbf{v}} - \sin\theta_{\mathbf{v}}\cos\phi_{\mathbf{v}})\right)\sin^2\left(\frac{\pi d_y}{\lambda_w}(\sin\vartheta_{\mathbf{v}}\sin\psi_{\mathbf{v}} - \sin\theta_{\mathbf{v}}\sin\phi_{\mathbf{v}})\right)}. \quad (11)\end{aligned}$$

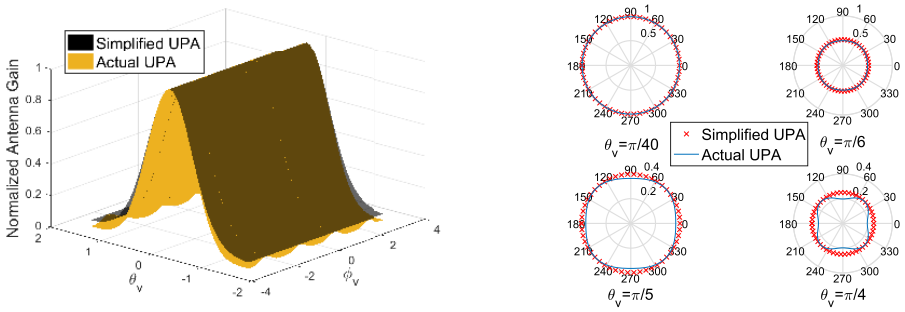

(a) Illustration of the simplified UPA and actual UPA. (b) Normalized antenna gain versus $\psi_{\mathbf{v}}$ with different $\theta_{\mathbf{v}}$.

Fig. 3. Comparison of the simplified UPA and actual UPA, with $\psi_{\mathbf{v}} = 0$, $\vartheta_{\mathbf{v}} = 0$, $2d_x = 2d_y = \lambda_w = \frac{3\times10^8\ m/s}{28\ GHz}$, $M_x = M_y = 2$, and for the simplified antenna pattern $\phi_c = \frac{\pi}{4}$.

2) Distribution of Interfering Distances: Assuming all horizontal distances between the typical user at the origin and other UAVs form a group $\{T_n\}_{n=1:N_v}$ with the realization $t_n = \|\mathbf{p}\|\ (\mathbf{p} \in \Phi/\mathbf{p}_0)$, where N_v is the number of the rest UAVs.

Note that the distributions of LOS and NLOS UAVs are two thinning processes of the parent points. If the interfering distance is t_n, the density for LOS and NLOS interferers are $p_L(\delta_{t_n})\lambda$ and $p_N(\delta_{t_n})\lambda$, respectively. The distribution of interfering distances can be figured out with the aid of the probability generating function of PPP [41] and we provide the detailed discussion in Appendix A.

B. Distance Distribution in i-th Nearest Scheme

If the typical user is the i-th nearest user to the typical UAV and the typical distance of such connection is u_i, the PDF of u_i can be derived by applying the i-th order statistic of these random variables [42], which is given by

$$f_i(u_i) = \frac{N!}{(i-1)!\,(N-i)!}\frac{u_i}{\sigma^2}\sum_{w=0}^{i-1}(-1)^{i-1-w}\binom{i-1}{w} \times \exp\left(-\frac{(N-w)\,u_i^2}{2\sigma^2}\right). \quad (18)$$

The difference of interfering distances between the RS scheme and the IN scheme is discussed in Lemma 1 and hence we omit it here.

IV. Performance Evaluation

In this section, we evaluate the SINR coverage and ASE performance of our clustered UAV networks based on the derived distance distributions.

A. Random Selection Scheme

In this scheme, the typical user is randomly selected from all intra-cluster users to ensure that each of them has the same opportunity to be served. The main merit of the RS scheme is that UAVs perform a fast response due to not acquiring other users' channel state information (CSI). This fair selection law has already been considered in other systems, e.g., *RNRF Selection Scheme* in NOMA networks [24], *Uniform Content Availability* [33] and *Uniform Distribution Model* [22] in D2D networks.

Before analyzing SINR coverage probabilities, we first derive *Laplace Transform of Interference* for tractability of the analysis. Considering an interfering UAV at $\mathbf{v} = (\mathbf{p}, h_v)$, the corresponding interfering distance $t_n = \|\mathbf{p}\|$ can be calculated by $t_n = \sqrt{r_P^2 + r_t^2 - 2r_P r_t\cos(\theta_P - \theta_t)}$, where $r_P = \|\mathbf{p} - \mathbf{p}_0\|$ is the distance between the serving UAV and the interfering UAV. $r_t = \|\mathbf{p}_0\|$ is the distance between the typical user and the serving UAV. $\theta_t = \angle(-\mathbf{p}_0)$ and $\theta_P = \angle(\mathbf{p} - \mathbf{p}_0)$. Note that t_n depends on four independent variables, namely r_P, r_t, θ_P, and θ_t. It is intractable to derive exact PDF of t_n. Fortunately, as the area of the considered ground plane approaches infinity, we are capable of proposing the following lemma.

Lemma 1: If the considered ground plane is $\mathbb{O} \subset \mathbb{R}^2$ and the area of $\mathbb{O}$ is infinity. The PDF of any actual interfering distance $f_{t_n}(t_n)$ and the PDF of the distance between the serving UAV and the interfering UAV $f_{r_P}(r_P)$ obeys that

$$\lim_{|\mathbb{O}|\to\infty} f_{t_n}(t_n) = f_{r_P}(r_P). \quad (19)$$

Proof: Assuming $\mathbb{O}$ is a circle with a radius R and the PDF of r_t is $f_{r_t}(r_t)$, we have $f_{r_P}(r_P) = \frac{2r_P}{R^2}$, $(0 \le r_P \le R)$, $f_{r_t}(r_t) = f_{RS}(r_t)$ for the RS scheme, and $f_{r_t}(r_t) = f_i(r_t)$ for the IN scheme. Note that $|r_P - r_t| \le t_n \le r_P + r_t$. Therefore, if $|r_P - r_t|$ and $r_P + r_t$ have the same PDF as $f_{r_P}(r_P)$, we are able to prove that r_t has negligible impact on t_n and hence t_n has the same distribution with r_P. For $z_1 = r_P + r_t$, since r_P and r_t are two independent variables, the PDF of z_1 is given by

$$f_{z_1}(z_1) = \int_0^\infty f_{r_t}(r_t) f_{r_P}(z_1 - r_t)dr_t = \frac{2z_1}{R^2} - \frac{2}{R^2}\int_0^\infty r_t f_{r_t}(r_t)dr_t \overset{(a)}{\to} \frac{2z_1}{R^2}, \quad (20)$$

where (a) follows the fact that $R \to \infty$ and the integral is a constant for both RS and IN scheme. For $z_2 = |r_P - r_t|$,

we first discuss the probability that $r_P < r_t$:

$$\mathbb{P}\left[r_t > r_P\right] = \int_0^{\infty} f_{r_t}\left(r_t\right) \int_0^{r_t} f_{r_P}\left(r_P\right) dr_P dr_t = \int_0^{\infty} \frac{x^2}{R^2} f_x\left(x\right) dx \overset{(a)}{\to} 0, \tag{21}$$

where $\mathbb{P}[.]$ is a probability function. Therefore, r_P is larger than r_t. Then, the PDF of $z_2 = r_P - r_t$ can be expressed as follows

$$f_{z_2}(z_2) = \int_0^{\infty} f_{r_t}(r_t) f_{r_P}(z_2 + r_t) dr_t = \frac{2z_2}{R^2} + \frac{2}{R^2} \int_0^{\infty} r_t f_{r_t}\left(r_t\right) dr_t \overset{(a)}{\to} \frac{2z_2}{R^2}. \tag{22}$$

From (20) *and* (22)*, we obtain that* $\lim_{R\to\infty} f_{z_1}(z_1) = \lim_{R\to\infty} f_{z_2}(z_2) = f_{r_P}(r_P)$*. For other shapes of the ground plane, the proof process is similar and hence we omit it here.* ∎

Remark 2: Based on **Lemma 1***, we conclude that the interference impact on different user selection schemes are the same when the ground plane has an infinite area.*

1) Laplace Transform of Interference: From the perspective of the typical user, interfering transmitters are all UAVs except the typical UAV. Therefore we only concentrate on inter-cluster interference.

Lemma 2: Assuming the inter-cluster interference is denoted by s, when $\alpha_\kappa \neq 2$ the Laplace transform of s is given by

$$\mathcal{L}\left(s\right) = \exp\Big(-2\lambda \sum_{\delta_{t_n} \in \mathbb{Z}^*} \int_0^1 \int_0^{\pi} \sum_{\kappa \in \{L,N\}} p_\kappa(\delta_{t_n}) \times \mathcal{G}_I^{\kappa}\left(\phi_{\mathbf{v}}, \omega, s\right) d\phi_{\mathbf{v}} d\omega \Big), \tag{23}$$

where

$$\mathcal{G}_I^{\kappa}\left(\phi_{\mathbf{v}}, \omega, s\right) = \mathrm{Z}_\kappa\left(\sqrt{a^2 + \hat{h}^2}, \frac{sC_\kappa \mathcal{G}\left(\phi_{\mathbf{v}}, \omega\right)}{N_L}\right) - \mathrm{Z}_\kappa\left(\sqrt{b^2 + \hat{h}^2}, \frac{sC_\kappa \mathcal{G}\left(\phi_{\mathbf{v}}, \omega\right)}{N_L}\right), \tag{24}$$

$$\mathrm{Z}_\kappa\left(A, \hat{s}\right) = \frac{A^2}{2}\left({}_2F_1\left(-\frac{2}{\alpha_\kappa}, N_\kappa; 1 - \frac{2}{\alpha_\kappa}; -\frac{\hat{s}}{A^{\alpha_\kappa}}\right) - 1\right), \tag{25}$$

$a = \delta_{t_n}/\sqrt{\lambda_a \lambda_b}$, and $b = (\delta_{t_n} + 1)/\sqrt{\lambda_a \lambda_b}$. $\mathbb{Z}^*$ is the set of non-negative integers, namely $\mathbb{Z}^* = \{0, 1, 2, \ldots\}$. ${}_2F_1(.)$ is Gauss hypergeometric function.

When $\alpha_N \neq 2$ and $\alpha_L = 2$, the Laplace transform of s is as follows:

$$\mathcal{L}\left(s\right) = \exp\Big(-2\lambda \sum_{\delta_{t_n} \in \mathbb{Z}^*} \int_0^1 \int_0^{\pi} \big(p_L(\delta_{t_n}) \mathcal{G}_{I_2}^{L}\left(\phi_{\mathbf{v}}, \omega, s\right) + p_N(\delta_{t_n}) \mathcal{G}_I^{N}\left(\phi_{\mathbf{v}}, \omega, s\right)\big) d\phi_{\mathbf{v}} d\omega \Big), \tag{26}$$

where

$$\mathcal{G}_{I_2}^{L}\left(\phi_{\mathbf{v}}, \omega, s\right) = \frac{sC_L \mathcal{G}\left(\phi_{\mathbf{v}}, \omega\right)}{2N_L} \Big(F_s\Big(\frac{sC_L \mathcal{G}\left(\phi_{\mathbf{v}}, \omega\right)}{N_L(b^2 + \hat{h}^2)}\Big) - F_s\Big(\frac{sC_L \mathcal{G}\left(\phi_{\mathbf{v}}, \omega\right)}{N_L(a^2 + \hat{h}^2)}\Big)\Big), \tag{27}$$

$$F_s\left(z\right) = N_L \ln\left(1 + \frac{1}{z}\right) + \frac{(z+1)^{N_L - 1} - 1}{z(z+1)^{N_L - 1}} - \sum_{m=\min(1, N_L - 1)}^{N_L - 1} \frac{\mathbf{U}(N_L - 2) N_L}{(z+1)^{N_L - m}\left(N_L - m\right)} \tag{28}$$

and $\mathbf{U}(.)$ is the unit step function.

Proof: See Appendix A. ∎

Note that Rayleigh fading channels, namely $N_L = 1$, are not suitable for modeling LOS transmission as it is most applicable in no dominant propagation scenarios. Therefore, we only consider $N_L > 1$ for analyzing the LOS scenarios.

This single-tier interference model can be extended to a general case with multiple independent interfering sources effortlessly. For example, if interfering BSs are modeled according to a PPP with a density λ_{BS} [27], the Laplace transform of interference for this general case is changed to $\mathcal{L}_g(s) = \mathcal{L}(s)\mathcal{L}_{BS}(s)$, where $\mathcal{L}_{BS}(s) = \mathcal{L}(s)|_{\lambda \to \lambda_{BS}}$ and $\lambda \to \lambda_{BS}$ means that λ is changed to λ_{BS}. For simplicity, we only consider this single-tier model in this paper.

Special case 1: In suburban environment, namely the product of λ_b and λ_a is small, the interval of steps $(1/\sqrt{\lambda_a \lambda_b})$ in (2) is expanded. As a result, the majority of interference should be LOS. We ignore all NLOS interference and the simplified antenna pattern in (13) is applied in this special case.

Corollary 1: Based on **Lemma 2**, the closed-form Laplace transform of interference $\tilde{\mathcal{L}}\left(s\right)$ for suburban environment can be expressed as

$$\tilde{\mathcal{L}}\left(s\right) = \exp\Big(-\frac{\pi^2 \lambda}{n_1} \sum_{\delta_{t_n} \in \mathbb{Z}^*} p_L(\delta_{t_n}) \times \sum_{i_1 = 1}^{n_1} \mathcal{G}_\Lambda^{L}\left(\phi_c, \frac{\zeta_{i_1} + 1}{2}, s\right) \sqrt{1 - \zeta_{i_2}^2} \Big), \tag{29}$$

where $\Lambda \in \{I, I_2\}$ represent conditions $\alpha_L \neq 2$ and $\alpha_L = 2$, respectively. The Gauss-Chebyshev node is $\zeta_{i_1} = \cos\left(\frac{2i_1 - 1}{2n_1}\pi\right)|_{i_1 = 1, 2, \ldots, n_1}$, where n_1 is the parameter balancing the accuracy and the complexity of this Gauss hypergeometric function [24]. The equality is established when $n_1 \to \infty$.

Proof: Based on the assumption in the special case 1, we delete NLOS interference part from (23) *and* (26) *to obtain* (29)*.* ∎

Remark 3: When the transmission distance increases, the received signal power decreases rapidly in mmWave communications, we are able to use first three LOS tiers, namely $\delta_{t_n} = 0, 1, 2$, to replace the whole considered area ($\delta_{t_n} \in \mathbb{Z}^*$) in the special case 1 for simplifying calculations.

2) Coverage Probability: To support demanded quality of services in the considered networks, one targeted data rate R_t is pre-decided for guaranteeing the communication. With the aid of Shannon-Hartley theorem, we have a SINR threshold $\Upsilon_{th} = (2^{R_t/B_w} - 1)$ in our system, where B_w is the bandwidth per resource block. The coverage probability is defined as the percentage of the received SINR at the typical user exceeding Υ_{th}, so it can be expressed as

$$P_{RS}\left(\Upsilon_{th}\right) = \mathbb{P}\left[\Upsilon\left(u\right) > \Upsilon_{th}, u = \|\mathbf{p}_0\|\right]. \tag{30}$$

Based on the Laplace transform of interference expressions in **Lemma 2** and **Corollary 1**, we obtain the coverage probability for the RS scheme.

Theorem 1: In the RS scheme, the typical user is randomly selected from all users in the typical cluster. The typical distance from the typical UAV at $\mathbf{v}_0$ to the typical user is $u = \|\mathbf{p}_0\|$. Therefore the SINR coverage probability is given by

$$\begin{aligned} &P_{RS}(\Upsilon_{th}) \\ &\approx \frac{\pi}{2n_2\sqrt{\lambda_a\lambda_b}} \sum_{i_2=1}^{n_2} \sqrt{1-\zeta_{i_2}^2} \sum_{\delta_u \in \mathbb{Z}^*} \sum_{\kappa \in \{L,N\}} p_\kappa(\delta_u) \\ &\quad \times \sum_{n_\kappa=1}^{N_\kappa} (-1)^{n_\kappa+1} \binom{N_\kappa}{n_\kappa} \Psi_\kappa\left(\frac{\zeta_{i_2}+2\delta_u+1}{2\sqrt{\lambda_a\lambda_b}}\right), \end{aligned} \tag{31}$$

where

$$\begin{aligned} \Psi_\kappa\left(u\right) = \exp\Big(-\frac{n_\kappa \eta_\kappa \Upsilon_{th}\sigma_n^2}{C_\kappa(u^2+\hat{h}^2)^{-\frac{\alpha_\kappa}{2}}}\Big) \\ \times \mathcal{L}\Big(\frac{n_\kappa \eta_\kappa \Upsilon_{th}}{C_\kappa(u^2+\hat{h}^2)^{-\frac{\alpha_\kappa}{2}}}\Big) f_{RS}\left(u\right) \end{aligned} \tag{32}$$

and $\eta_\kappa = N_\kappa (N_\kappa!)^{-\frac{1}{N_\kappa}}$.

Proof: See Appendix B. ∎

Remark 4: Regarding the normalized antenna gain $\mathcal{G}(\phi_{\mathbf{v}}, \omega)$ *in* (12)*, the expectation of this antenna gain is a monotonic decreasing function with* M*. With the aid of* (A.3) *and* **Lemma 2***, we find that* $\mathcal{L}\left(\frac{n_\kappa \eta_\kappa \Upsilon_{th}}{C_\kappa\left(u^2+\hat{h}^2\right)^{-\frac{\alpha_\kappa}{2}}}\right)$ *has a positive correlation with* M*. Therefore, the coverage probability in* **Theorem 1** *is a monotonic increasing function with* M*.*

Remark 5: Note that $\sigma_n^2 = \frac{|n_0|^2}{PM}$*. Since the diversity order of* P_{RS} *in terms of the transmit signal-to-noise ratio (SNR)* $\frac{P}{|n_0|^2}$ *obeys that* $\mathrm{d}_{RS} = \lim\limits_{P/|n_0|^2 \to \infty} \frac{\log P_{RS}}{\log(P/|n_0|^2)} = \lim\limits_{\sigma_n^2 \to 0} \frac{\log P_{RS}}{\log(P/|n_0|^2)} = 0$*,* P_{RS} *has an upper bound, which is called the error floor. For high SNR scenarios when* $\frac{P}{|n_0|^2} \to \infty$*, the error floor of* P_{RS} *is given by*

$$\lim_{P/|n_0|^2 \to \infty} P_{RS} = P_{RS}\Big|_{\Psi_\kappa(u) \to \mathcal{L}\left(\frac{n_\kappa \eta_\kappa \Upsilon_{th}}{C_\kappa(u^2+\hat{h}^2)^{-\frac{\alpha_\kappa}{2}}}\right) f_{RS}(u)}. \tag{33}$$

It is worth noting that this error floor ignores the noise effects, which means it also represents the coverage performance under interference-limited scenarios.

Corollary 2: In the suburban environment as described in the special case 1, the closed-form expressions for coverage probabilities in the RS scheme is

$$\begin{aligned} &\tilde{P}_{RS}\left(\Upsilon_{th}\right) \\ &\approx \frac{\pi}{2n_2\sqrt{\lambda_a\lambda_b}} \sum_{i_2=1}^{n_2} \sqrt{1-\zeta_{i_2}^2} \sum_{\delta_u \in \mathbb{Z}^*} \\ &\quad \times p_L\left(\delta_u\right) \sum_{n_L=1}^{N_L} (-1)^{n_L+1} \binom{N_L}{n_L} \tilde{\Psi}_L\left(\frac{\zeta_{i_2}+2\delta_u+1}{2\sqrt{\lambda_a\lambda_b}}\right), \end{aligned} \tag{34}$$

where

$$\begin{aligned} \tilde{\Psi}_L\left(u\right) = \exp\Big(-\frac{n_L \eta_L \Upsilon_{th}\sigma_n^2}{C_L(u^2+\hat{h}^2)^{-\frac{\alpha_L}{2}}}\Big) \\ \times \tilde{\mathcal{L}}\Big(\frac{n_L \eta_L \Upsilon_{th}}{C_L(u^2+\hat{h}^2)^{-\frac{\alpha_L}{2}}}\Big) f_{RS}\left(u\right). \end{aligned} \tag{35}$$

Proof: When considering the special case 1, we are able to use (29) *to replace* (26) *and the NLOS part in* (3) *can be deleted from* **Theorem 1**. ∎

In practical scenarios, most UAV networks with mmWave communications suits the special case 1, even though we assume such special case is valid in suburban environment. For example, authors in [28] proposed a urban blockage setting, where $\epsilon = 20$ m $\lambda_a = 0.5$ and $\lambda_b = 300 \times 10^{-6}$ m^{-2}. Thus the interval of the transmission distance r in equation (2) is $1/\sqrt{\lambda_a\lambda_b} \approx 80$ m, which means if the served user is located within this range $[0, 80)$ m, the corresponding transmission is a LOS link due to $p_L(0) = 1$. Regarding the typical user in our work, it is normally located within the first LOS tier $\delta = 0$ due to the limited coverage ability of UAVs. Furthermore, since NLOS transmission experience more severe path loss compared with LOS transmission, the effects of NLOS interference are negligible for most mmWave networks [10], [22], [30], [43]. The equation in **Corollary 2** can be treated as the proxy of exact analysis expressions in the rest of this paper and demonstrations are provided in Section V.

In several research works [10], [30], [44], due to the large bandwidth, mmWave communications in sparse networks, where the density of interferers is small, are regarded as noise-limited systems. Therefore, we propose a special case to analyze the performance of noise-limited scenarios.

Special case 2: The considered network is a noise-limited system, namely $\mathcal{L}(.) = 1$.

Corollary 3: In the noise-limited system, the exact coverage probability can be expressed as

$$\begin{aligned} &\bar{P}_{RS}\left(\Upsilon_{th}\right) \\ &= \frac{\pi}{2n_2\sqrt{\lambda_a\lambda_b}} \\ &\quad \times \sum_{i_2=1}^{n_2} \sqrt{1-\zeta_{i_2}^2} \sum_{\delta_u \in \mathbb{Z}^*} p_L(\delta_u) \bar{\Psi}_L\Big(\frac{\zeta_{i_2}+2\delta_u+1}{2\sqrt{\lambda_a\lambda_b}}\Big), \end{aligned} \tag{36}$$

where

$$\bar{\Psi}_L\left(u\right) = \left(1 - \frac{\gamma\Big(N_L, \frac{N_L \Upsilon_{th}\sigma_n^2}{C_L(u^2+\hat{h}^2)^{-\frac{\alpha_L}{2}}}\Big)}{(N_L-1)!}\right) f_{RS}\left(u\right) \tag{37}$$

and $\gamma(s,x) = \int_0^x t^{s-1}\exp\left(-t\right)dt$ is the lower incomplete gamma function.

Proof: See Appendix C. ∎

Remark 6: Since $\bar{P}_{RS}(0) = \bar{P}_{RS}(\infty) = 0$ *and* $\bar{P}'_{RS}(h_v) = \frac{d\bar{P}_{RS}(h_v)}{dh_v}$ *does not constantly equal to* 0*, there exists at least one extremum for* $\bar{P}_{RS}(h_v)$*. Additionally,* $\bar{P}_{RS}(h_v) \geq 0$ *in the range* $h_v \in [0, \infty)$*, we obtain that the extremum is the maximum for* $\bar{P}_{RS}(h_v)$*. Therefore, the trade-off between the high LOS probability and the short actual transmission distance contributes to at least one optimal value of* h_v*, which is capable of maximizing the coverage probability in* (36)*.*

B. i-th Nearest Scheme

It is worth noting that in the RS scheme, only the randomly selected user's performance can be evaluated. To analyze the performance of each user in a cluster, we propose the IN scheme. Based on this scheme, several further actions of UAVs can be executed, e.g., power allocations, digital precoding, analog beamforming, and so forth. These interesting topics will be studied in our future work.

Two schemes have the same Laplace transform of interference as provided in **Lemma 2** and **Corollary 1**. Based on such expressions we are able to derive the coverage probability for the IN scheme. Firstly, the coverage probability for the i-th closest typical user at $\mathbf{u}_i = (\mathbf{d}_i, h_u)$ in the typical cluster is defined as

$$P^i_{IN}(\Upsilon_{th}) = \mathbb{P}\left[\Upsilon(u_i) > \Upsilon_{th}, u_i = \|\mathbf{p}_0 - \mathbf{d}_i\|\right]. \quad (38)$$

With the aid of (2) and (18), the coverage probability for the i-th closest user can be calculated in the following theorem.

Theorem 2: The i-th closest user to the typical UAV is selected as the typical user, which has a communication distance u_i. The coverage probability for the typical user in the IN scheme is given by

$$\begin{aligned} &P^i_{IN}(\Upsilon_{th}) \\ &\approx \frac{\pi}{2n_2\sqrt{\lambda_a\lambda_b}} \sum_{i_2=1}^{n_2} \sqrt{1-\zeta_{i_2}^2} \sum_{\delta_{u_i}\in\mathbb{Z}^*} \\ &\quad \sum_{\kappa\in\{L,N\}} p_\kappa(\delta_{u_i}) \sum_{n_\kappa=1}^{N_\kappa} (-1)^{n_\kappa+1} \binom{N_\kappa}{n_\kappa} \Psi^i_\kappa\Big(\frac{\zeta_{i_2}+2\delta_{u_i}+1}{2\sqrt{\lambda_a\lambda_b}}\Big), \end{aligned} \quad (39)$$

where

$$\begin{aligned} \Psi^i_\kappa(u_i) = \exp\left(-\frac{n_\kappa\eta_\kappa\Upsilon_{th}\sigma_n^2}{C_\kappa(u_i^2+\hat{h}^2)^{-\frac{\alpha_\kappa}{2}}}\right) \\ \times\mathcal{L}\left(\frac{n_\kappa\eta_\kappa\Upsilon_{th}}{C_\kappa(u_i^2+\hat{h}^2)^{-\frac{\alpha_\kappa}{2}}}\right) f_i(u_i). \end{aligned} \quad (40)$$

Proof: With the similar proof procedure of **Theorem 1***, we replace* $f_{RS}(.)$ *by* $f_i(.)$ *to derive this theorem.* ∎

Remark 7: Due to obtaining stronger received power, the nearer user has higher coverage performance, which means $P^1_{IN} > P^2_{IN} > \ldots > P^N_{IN}$*. It is worth noting that* $\sum_{i=1}^{N} f_i(r)/N = f_{RS}(r)$ *and hence* $\sum_{i=1}^{N} P^i_{IN}/N = P_{RS}$*. As a result, we have* $P^1_{IN} > P_{RS} > P^N_{IN}$ *when* $N > 1$*. In other words, the performance of the RS scheme is between the best and worst case in the IN scheme.*

Remark 8: Similar with **Remark 5***, we obtain that the diversity order of* P^i_{IN} *in terms of* $\frac{P}{|n_0|^2}$ *is also zero. For high SNR scenarios, the error floor of* P^i_{IN} *can be expressed as*

$$\lim_{P/|n_0|^2\to\infty} P^i_{IN} = P^i_{IN}\Big|_{\Psi^i_\kappa(u_i)\mapsto\mathcal{L}\left(\frac{n_\kappa\eta_\kappa\Upsilon_{th}}{C_\kappa(u_i^2+\hat{h}^2)^{-\frac{\alpha_\kappa}{2}}}\right) f_i(u_i)}. \quad (41)$$

As discussed in **Remark 5***, this error floor is also the expression for interference-limited scenarios under the IN scheme.*

Remark 9: Since the Laplace transform of interference in **Lemma 2** *is a monotonic decreasing function in terms of the UAV density* λ*, the coverage probabilities for two proposed schemes, namely* P_{RS} *and* P_{IN}*, are inversely proportional to* λ*. When* λ *increases, the number of interferers enlarges and hence the considered system becomes interference-limited. Moreover, if* $\lambda \to \infty$*,* $P_{RS}, P_{IN} \to 0$*. As a conclusion, to guarantee the required quality of service in interference-limited UAV networks, efficient interference cancellation techniques are needed.*

Corollary 4: Under the special case 1, we ignore all NLOS transmission. Therefore, the closed-form coverage probability in the IN scheme is given by

$$\begin{aligned} &\tilde{P}^i_{IN}(\Upsilon_{th}) \\ &\approx \frac{\pi}{2n_2\sqrt{\lambda_a\lambda_b}} \sum_{i_2=1}^{n_2} \sqrt{1-\zeta_{i_2}^2} \sum_{\delta_{u_i}\in\mathbb{Z}^*} p_L(\delta_{u_i}) \\ &\quad \times \sum_{n_L=1}^{N_L} (-1)^{n_L+1} \binom{N_L}{n_L} \tilde{\Psi}^i_L\left(\frac{\zeta_{i_2}+2\delta_{u_i}+1}{2\sqrt{\lambda_a\lambda_b}}\right), \end{aligned} \quad (42)$$

where

$$\begin{aligned} \tilde{\Psi}^i_\kappa(u_i) = \exp\left(-\frac{n_\kappa\eta_\kappa\Upsilon_{th}\sigma_n^2}{C_\kappa(u_i^2+\hat{h}^2)^{-\frac{\alpha_\kappa}{2}}}\right) \\ \times\tilde{\mathcal{L}}\left(\frac{n_\kappa\eta_\kappa\Upsilon_{th}}{C_\kappa(u_i^2+\hat{h}^2)^{-\frac{\alpha_\kappa}{2}}}\right) f_i(u_i). \end{aligned} \quad (43)$$

Proof: The proof procedure is similar with that in ***Corollary 2*** and hence we omit it. ∎

Corollary 5: In the noise-limited system as discussed in the special case 2, the interference part can be removed from the coverage probability in **Corollary 4**. Therefore the exact coverage probability is given by

$$\begin{aligned} &\bar{P}^i_{IN}(\Upsilon_{th}) = \frac{\pi}{2n_2\sqrt{\lambda_a\lambda_b}} \\ &\quad \times \sum_{i_2=1}^{n_2} \sqrt{1-\zeta_{i_2}^2} \sum_{\delta_u\in\mathbb{Z}^*} p_L(\delta_u) \bar{\Psi}^i_L\Big(\frac{\zeta_{i_2}+2\delta_u+1}{2\sqrt{\lambda_a\lambda_b}}\Big), \end{aligned} \quad (44)$$

where

$$\bar{\Psi}^i_L(u_i) = \left(1 - \frac{\gamma\Big(N_L, \frac{N_L\Upsilon_{th}\sigma_n^2}{C_L(u_i^2+\hat{h}^2)^{-\frac{\alpha_L}{2}}}\Big)}{(N_L-1)!}\right) f_i(u_i). \quad (45)$$

Proof: With the aid of the similar proof method in **Corollary 4** *and the distance distribution in* (18)*, we obtain this corollary.* ∎

Since UAV networks are still at the design stage, the actual distribution of UAV's altitude is unknown. Therefore, we assume all UAVs are hovering at the same height of h_v. For a more general case with an altitude distribution of UAVs $p_h(h_v)$, the final coverage probability can be effortlessly derived with the aid of our expressions, which is as follows:

$$P_{cov}(\Upsilon_{th}) = \int_0^\infty f_{cov}(\Upsilon_{th}, h_v) p_h(h_v) dh_v, \tag{46}$$

where $f_{cov} \in \{P_{RS}, \tilde{P}_{RS}, \bar{P}_{RS}, P_{IN}^i, \tilde{P}_{IN}^i, \bar{P}_{IN}^i\}$.

The proposed system considers the scenario that all intra-cluster users have the same priority. In the typical cluster, if one of the intra-cluster users is the primary user that needs the best channel conditions, it is better to assume the UAV flies towards this primary user and then hover above its head to transmit messages. We proposed another special case to describe this situation.

Special case 3: In the typical cluster, the typical user is the primary user and hence the serving UAV hovers above its head to transmit information.

Corollary 6: Under the special case 3, both the RS and IN schemes have the same coverage probabilities, which are as follows:

$$\begin{aligned} P_{s3}(\Upsilon_{th}) &\approx \sum_{\delta_u \in \mathbb{Z}^*} \sum_{\kappa \in \{L,N\}} p_\kappa(\delta_u) \sum_{n_\kappa=1}^{N_L} (-1)^{n_L+1} \\ &\times \binom{N_L}{n_L} \exp\Big(-\frac{n_L \eta_L \Upsilon_{th} \sigma_n^2}{C_L \hat{h}^{-\alpha_L}}\Big) \mathcal{L}\Big(\frac{n_L \eta_L \Upsilon_{th}}{C_L \hat{h}^{-\alpha_L}}\Big), \end{aligned} \tag{47}$$

Proof: Note that the desired communication distance under special case 3 is fixed as $\hat{h}$. By replacing $\sqrt{u^2+h_v^2}$ in **Theorem 1** *and $\sqrt{u_i^2+h_v^2}$ in* **Theorem 2** *with the constant $\hat{h}$, we obtain this corollary.* ∎

C. Area Spectral Efficiency

Depending on the coverage probability, we are able to derive ASE. The ASE is defined as the average rate per unit area and unit bandwidth. This parameter helps to optimize the desired data rate at the user side and the density of UAVs for maximizing the spectral efficiency with considering the spatial factor. The expression of ASE is given by

$$ASE = \lambda_{ase} \log_2(1+\Upsilon_{th}) P_c, \tag{48}$$

where λ_{ase} is the average number of users in an unit area and P_c is the coverage probability.

Based on the coverage probability as discussed earlier for the proposed two user selection schemes, we obtain the following proposition in terms of ASE.

Proposition 1: ASE for two user selection schemes, namely the RS scheme and the IN scheme, can be expressed as

$$ASE = N\lambda \log_2(1+\Upsilon_{th}) P_c(\Upsilon_{th}), \tag{49}$$

where $P_c \in \{P_{RS}, P_{IN}^i\}$ is the coverage probability for universal scenarios, $P_c \in \{\tilde{P}_{RS}, \tilde{P}_{IN}^i\}$ is the coverage probability for the special case 1, $P_c \in \{\bar{P}_{RS}, \bar{P}_{IN}^i\}$ is the coverage probability for the special case 2, and $P_c = P_{s3}$ is the coverage probability for the special case 3.

Remark 10: In (49)*, large density λ increases area efficiency, but it decreases the coverage probability due to incurring more interference. Additionally, a large SINR threshold Υ_{th} contributes to fast data rates but it impairs the corresponding coverage probability $P_c(\Upsilon_{th})$. As a result, optimal λ and Υ_{th} are existed in our system for maximizing ASE.*

V. Numerical Results

We state the general parameters of the proposed networks in Table II [10], [22], [28], [30]. The transmit power P is assumed to be 1 W. In terms of the intercept, the reference distance d_0 for both LOS and NLOS path loss laws is assumed to be one meter, which ensures $C_L = C_N = \left(\frac{\lambda_w}{4\pi d_0}\right)^2$. MC simulations include LOS links, NLOS links, noise, and actual interfering communication distances. As shown in Fig. 4(a), coverage probabilities with interfering distances t_n and r_P have the same value, which validates **Remark 2**. Moreover, tight approximation expressions in **Theorem 1** and **Theorem 2** match the MC simulations with a negligible difference. Regarding the square UPA, if we apply $\phi_c = \frac{\pi}{4}$ for the simplified UPA, interference is overestimated. Fig. 4(a) illustrates that this flaw can be overcome by applying a value between 0 and $\frac{\pi}{4}$.

Verifications of special cases are illustrated in Fig. 4(b). For the special case 1, when the density of buildings is small, namely in suburban environment, tight approximations in **Corollary 2** and **Corollary 4** fit the MC simulations ideally. For the special case 2, when the bandwidth $B_w = 2$ GHz and the density of UAVs $\lambda = 1/(2000^2\pi)$ m^{-2}, our network becomes a noise-limited system. Under this condition, exact expressions in **Corollary 3** and **Corollary 5** overlap with the SNR simulation results. When comparing with the MC simulations, the difference is also acceptable. When the density of UAVs increases, the proposed system becomes interference-limited and the expressions provided in **Remark 5** and **Remark 8** are able to represent this coverage performance. Additionally, high UAV densities rapidly weaken the performance due to introducing severe interference and hence efficient interference cancellation techniques are essential as mentioned in **Remark 9**.

In traditional cellular networks, the average height of macro BSs in urban scenarios is around 30 m. Compared with the macro BSs, UAVs are able to adjust their altitude for enhancing the communications. Fig. 5(a) demonstrates that for SINR scenarios, there exists an optimal value of height in the considered environment to maximize the coverage probability in UAV networks. This property is similar to SNR scenarios as discussed in **Remark 6**. All of the optimal heights unequal to 30 m, which means UAV networks outperform the traditional cellular networks by amending the altitude of transmitters.

In the IN scheme, as discussed in **Remark 7**, Fig. 5(a) shows that the best coverage probability $P_{IN}^1(\Upsilon_{th})$ and the worst coverage probability $P_{IN}^N(\Upsilon_{th})$ performs better and worse than that in the RS scheme, respectively. In terms of $\lambda_a \lambda_b$, which represent the density of buildings, sparse

TABLE II
GENERAL SETTINGS OF NETWORKS

Carrier frequency	$f_m = 28$ GHz	**Density of PPP**	$\lambda = 1/(250^2\pi)$ m^{-2}
Path loss law for LOS	$\alpha_L = 2$, $N_L = 3$	**Path loss law for NLOS**	$\alpha_N = 4$, $N_N = 2$
Number of antennas	$M_x = M_y = 2$	**Antenna parameter**	$\lambda_w = 2d_x = 2d_y$
Standard deviation	$\sigma = 20$	**Number of users each cluster**	$N = 6$
Altitude	$h_u = 0$ m, $h_v = 50$ m	**Bandwidth per resource block**	$B_w = 100$ MHz
Building density	$\lambda_a = 0.1$, $\lambda_b = 10 \times 10^{-6}$	**Scale parameter for buildings**	$\epsilon = 20$ m

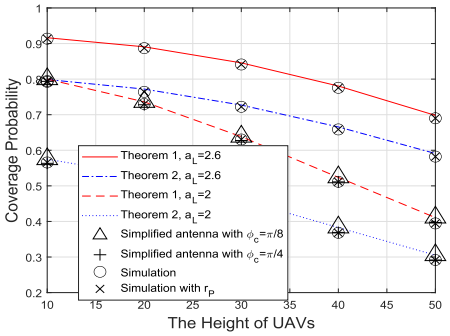

(a) Coverage probability versus the height of UAVs h_v, with $N_L = 2$, $N_N = 1$, $i = N$ for IN scheme, and the pre-decided threshold $\Upsilon_{th} = 10$ dB.

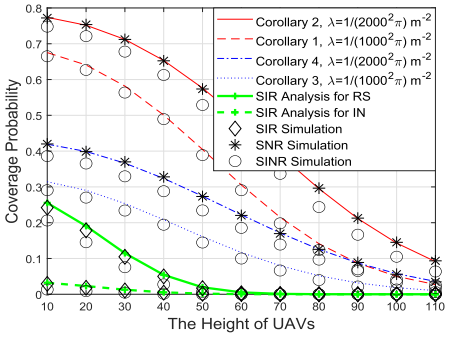

(b) Coverage probability versus the height of UAVs h_v, with $\phi_c = \frac{\pi}{8}$, $N_L = 2$, $N_N = 1$, $\sigma = 40$, $B_w = 2$ GHz, $i = N$ for IN scheme, and the pre-decided threshold $\Upsilon_{th} = 17$ dB. For SIR scenarios, the density of UAVs $\lambda = \frac{1}{300^2\pi}$ m^{-2}.

Fig. 4. Verifications with the aid of Monte Carlo simulations.

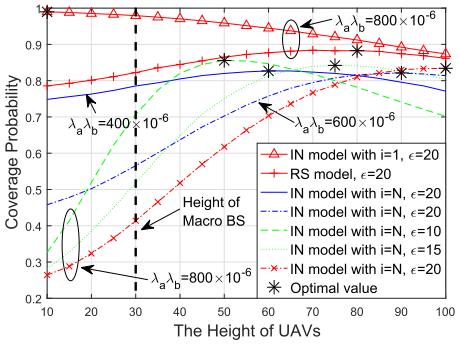

(a) Coverage probability versus the height of UAVs h_v, with the pre-decided threshold $\Upsilon_{th} = 10$ dB.

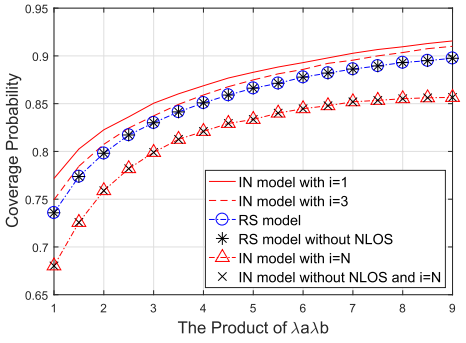

(b) Coverage probability versus the product of $\lambda_a\lambda_b$, with the pre-decided threshold $\Upsilon_{th} = 10$ dB.

Fig. 5. The impact of the UAVs altitude h_v and the environment of buildings.

building environment with $\lambda_a\lambda_b = 400 \times 10^{-6}$ m^{-2} achieves the highest coverage probability in low height regions. On the contrary, dense building environment with $\lambda_a\lambda_b = 800 \times 10^{-6}$ m^{-2} performs the best in high height regions. Lastly, with the increase of average height of buildings ϵ, the coverage probability gradually decreases.

We mentioned that ignoring NLOS transmission affects the coverage performance negligibly. Fig. 5(b) shows that coverage probabilities for only LOS transmission are nearly the same with actual results both in the RS scheme and IN scheme, thereby validating this remark. In the IN scheme, the close user has a high coverage probability. When the density of buildings $\lambda_a\lambda_b$ arises, the discrepancy between the best and the worst coverage probability enlarges.

In Table II, the density of PPP represents the density of UAVs, which is $1/(250^2\pi)$ m^{-2}. In this case, the horizontal coverage of UAVs is a circle with a radius of 250 m. Fig. 6(a) illustrates that the coverage probability has a positive correlation with such radius. Since bandwidth only affects the thermal noise, changing this parameter has no impact on signal-to-interference-ratio (SIR) coverage probabilities. With the rise of σ, the SIR coverage probability decreases. Regarding the SINR coverage performance, the impact of noise, namely the difference between SIR and SINR coverage probability, is enhanced by increasing the bandwidth and the coverage radius. As a result, in a dense network with small bandwidth, the proposed UAV network can be regarded as an interference-limited system. On the contrary, a noise-limited system can be achieved in a sparse network with large bandwidth.

As we employ the UPA antenna at UAVs, the number of elements in one UAV antenna arouses the interest of us. As shown in Fig. 6(b), the coverage probability is a monotonic increasing function with M as discussed in **Remark 4**. Furthermore, we investigate the number of users in one cluster as well. in the RS scheme, such number N has no effect in

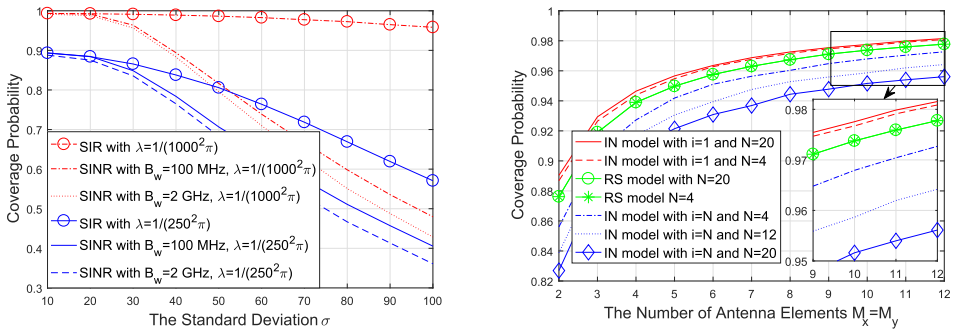

(a) Coverage probability versus the radius for the standard derivation of clusters for RS scheme, with $\lambda_a = 0.2$, $\lambda_b = 1000 \times 10^{-6}$, and $\Upsilon_{th} = 10$ dB.

(b) Coverage probability versus the number of elements for one UAV antenna, with $\lambda_a = 0.2$, $\lambda_b = 1000 \times 10^{-6}$, $B_w = 2$ GHz, and $\Upsilon_{th} = 10$ dB.

Fig. 6. The impact of the density of UAVs λ and the antenna scales M.

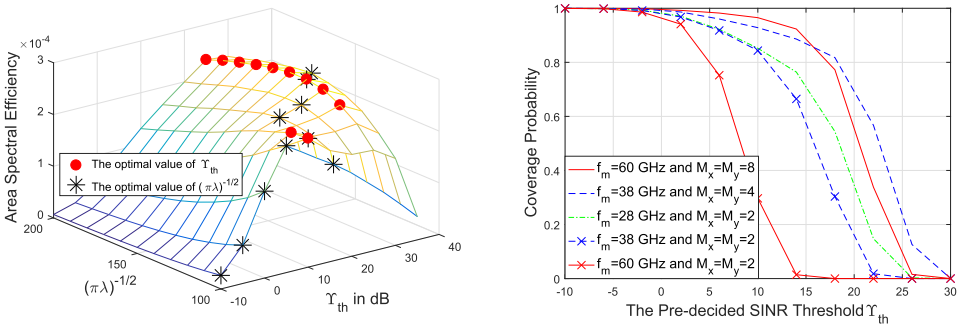

(a) Coverage probability versus the density of UAVs λ and the pre-decided SINR threshold Υ_{th} for RS scheme, with $\lambda_a = 0.5$, and $\lambda_b = 300 \times 10^{-6}$.

(b) Coverage probability versus the pre-decided SINR threshold Υ_{th} for RS scheme, with $\lambda_a = 0.5$, $\lambda_b = 300 \times 10^{-6}$, and $B_w = 2$ GHz.

Fig. 7. The performance of ASE and different carrier frequencies.

TABLE III

LOS AND NLOS PATH LOSS EXPONENTS FOR VARIOUS CARRIER FREQUENCIES

Carrier Frequencies	28G	38G	60G
LOS α_L	2	2	2.25
Strongest NLOS α_N	3	3.71	3.76
Number of antenna elements M	2×2	4×4	8×8

terms of the coverage probability. However, in the IN scheme, the large N impairs the performance of the worst coverage probability $P_{IN}^{N}(\Upsilon_{th})$, while it benefits the performance of the best coverage probability $P_{IN}^{1}(\Upsilon_{th})$.

Since the performance of ASE and different carrier frequencies for the IN scheme has the same properties with the counterpart in the RS scheme, we only present such performance in the RS scheme in this part. Fig. 7(a) illustrates that both the pre-decided SINR threshold Υ_{th} and the density of UAVs λ have the optimal value for achieving the maximum ASE as discussed in **Remark 10**. With the increase of Υ_{th}, the optimal value of λ decreases. Additionally, with the increase of λ, the optimal value of Υ_{th} also decreases.

There are numerous available carrier frequencies in mmWave communications. We present path loss exponents and approximated antenna scales for three typical carrier frequencies in Table III [22], [45], [46]. The performance is shown in Fig. 7(b). In order to compare a single variable, we fix the antenna scales as $M = 2 \times 2$ and the only variable

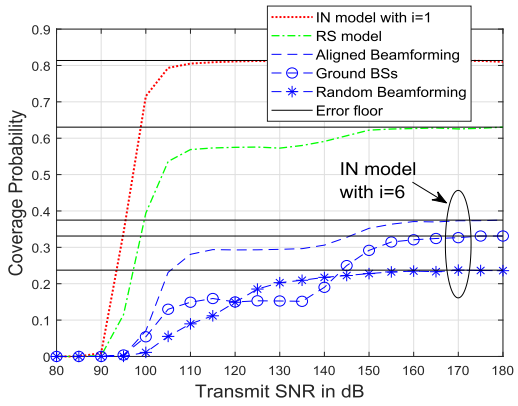

Fig. 8. Coverage probability versus transmit SNR $\frac{P}{|n_0|^2}$, with $M_x = M_y = 4$, $\lambda = 3/(250^2\pi)$, $\sigma = 60$, $\Upsilon_{th} = 10$ dB, $\lambda_a = 0.2$, $\lambda_b = 1000 \times 10^{-6}$.

is the path loss exponent. It is clear that 28 GHz is the best choice under this condition. Note that higher frequencies contribute to the smaller size of antenna elements and shorter antenna spacing [47]. To evaluate the antenna impact on different carrier frequencies, we provide different antenna sizes in Table III. From Fig. 7(b), we find that by increasing the number of antenna elements, 60 GHz outperform the other two carrier frequencies in low Υ_{th} regions and 38 GHz achieves the highest coverage probability in high Υ_{th} regions. The large antenna scale is able to compensate for the transmission loss for high frequencies.

In high SNR scenarios, Fig. 8 shows that the coverage probability of all user selection schemes, namely RS and IN, tends to an error floor as discussed in **Remark 5** and **Remark 8**. Compared with conventional wireless systems with random beamforming [48] and ground communications with BSs at 30 m [40], the proposed UAV network with aligned beamforming achieves higher coverage performance.

VI. Conclusion

This paper has investigated SINR coverage performance and ASE for clustered UAV networks with mmWave communications, where all users are modeled as a typical PCP and UAVs are located above each cluster centers with a fixed hight. The adjustable altitude of UAVs contributes to higher coverage probability compared with traditional cellular networks. With the aid of Laplace transform of interference, several closed-form expressions for the SINR coverage probability have been derived under two different user selection schemes. We have analytically demonstrated that large antenna scale is able to enhance the coverage performance. When the density of buildings is low and the bandwidth is large, our network can be regarded as a noise-limited system. On the contrary, the proposed network can be treated as an interference-limited system with a high density of buildings and small bandwidth. There exist optimal values of pre-decided SINR threshold and the density of UAVs to maximize ASE. If the antenna scale is fixed, 28 GHz is the best choice for the carrier frequency compared with 38 GHz and 60 GHz. However, high-frequency scenario is able to employ more elements in one antenna, which significantly boosts the coverage probability. Based on the proposed framework, our future work will focus on the design of hybrid precoding for MIMO-UAV systems.

Appendix A: Proof of Lemma 2

When $\alpha_\kappa \neq 2$, since there exists two kinds of interference ($I = \sum_{\mathbf{p}\in\Phi/\mathbf{p}_0} \mathrm{L}(\|\mathbf{p}\|)|h_\mathbf{v}|^2\mathcal{G}(\phi_\mathbf{v},\omega)$) from inter-cluster UAVs: interference with LOS transmission I_L and NLOS transmission I_N. We define the Laplace transform of interference as

$$\mathcal{L}(s) = \mathbb{E}[\exp(-sI)] = \underbrace{\mathbb{E}[\exp(-sI_L)]}_{\Theta_L}\underbrace{\mathbb{E}[\exp(-sI_N)]}_{\Theta_N}, \tag{A.1}$$

where $\mathbb{E}(.)$ is the expectation function and

$$I_\kappa = \sum_{\mathbf{p}\in\Phi\setminus\mathbf{p}_0} |h_\mathbf{v}|^2\mathcal{G}(\phi_\mathbf{v},\omega)\,\mathrm{L}(t_n)\mathbb{B}(p_\kappa(\delta_{t_n})), \quad (t_n = \|\mathbf{p}_n\|, \delta_{t_n} = \left\lfloor t_n\sqrt{\lambda_a\lambda_b}\right\rfloor). \tag{A.2}$$

By substituting (A.2) into (A.1), we first derive the Laplace transform of interference for LOS at the bottom of this page. In (A.3), (a) follows the method by substituting (3), (10) and (11) into (A.1). (b) is figuring out the expectation of Gamma random variable $|h_\mathbf{v}|^2$. (c) uses **Lemma 1**, the probability generating function of PPP [41] with density λ, and $\hat{s}(\phi_\mathbf{v},\omega,s) = sC_L\mathcal{G}(\phi_\mathbf{v},\omega)/N_L$.

Before deriving the closed-form express, we introduce an typical integral as [49]

$$\begin{aligned}\mathrm{Z}_\kappa(A,\hat{s}) &= \int_A^\infty \left(1-\left(1+\frac{\hat{s}}{y^{\alpha_\kappa}}\right)^{-N_\kappa}\right) y dy \\ &= \frac{A^2}{2}\left({}_2F_1\left(-\frac{2}{\alpha_\kappa}, N_\kappa; 1-\frac{2}{\alpha_\kappa}; -\frac{\hat{s}}{A^{\alpha_\kappa}}\right)-1\right),\end{aligned} \tag{A.4}$$

where ${}_2F_1(.)$ is the Gauss hypergeometric function. By substituting (A.4) into (A.3) we obtain

$$\begin{aligned}&\Theta_L \\ &= \exp\Big(-2\pi\lambda\sum_{\delta_{t_n}\in\mathbb{Z}^*} p_L(\delta_{t_n})\mathbb{E}_\mathcal{G}\Big[\mathrm{Z}_L\big(\sqrt{a^2+\hat{h}^2},\hat{s}(\phi_\mathbf{v},\omega,s)\big) \\ &\quad -\mathrm{Z}_L\big(\sqrt{b^2+\hat{h}^2},\hat{s}(\phi_\mathbf{v},\omega,s)\big)\Big]\Big) \\ &\overset{(d)}{=} \exp\Big(-2\lambda\sum_{\delta_{t_n}\in\mathbb{Z}^*} p_L(\delta_{t_n})\int_0^1\int_0^\pi \mathcal{G}_I^L(\phi_\mathbf{v},\omega,s)\,d\phi_\mathbf{v}d\omega\Big),\end{aligned} \tag{A.5}$$

where $\mathcal{G}_I^\kappa(\phi_\mathbf{v},\omega,s) = \mathrm{Z}_\kappa\big(\sqrt{a^2+\hat{h}^2},\hat{s}(\phi_\mathbf{v},\omega,s)\big) - \mathrm{Z}_\kappa\big(\sqrt{b^2+\hat{h}^2},\hat{s}(\phi_\mathbf{v},\omega,s)\big)$. (d) calculates the expectation of antenna gain with the aid of the fact that $\mathcal{G}(\phi_\mathbf{v},\omega)$ is a even function in terms of $\phi_\mathbf{v}$ and ω. With the similar proof procedure, the NLOS part is given by

$$\Theta_N = \exp\Big(-2\lambda\sum_{\delta_{t_n}\in\mathbb{Z}^*}(1-p_L(\delta_{t_n})) \times\int_0^1\int_0^\pi \mathcal{G}_I^N(\phi_\mathbf{v},\omega,s)d\phi_\mathbf{v}d\omega\Big). \tag{A.6}$$

$$\begin{aligned}\Theta_L &\overset{(a)}{=} \mathbb{E}\left[\exp\left(-s\sum_{\mathbf{p}\in\Phi\setminus\mathbf{p}_0}|h_\mathbf{v}|^2\mathcal{G}(\phi_\mathbf{v},\omega)\,C_L\left(t_n^2+\hat{h}^2\right)^{-\frac{\alpha_L}{2}}\right)\right] \\ &\overset{(b)}{=} \mathbb{E}_\mathcal{G}\left[\prod_{\mathbf{p}\in\Phi\setminus\mathbf{p}_0}\mathbb{E}_\mathbf{p}\left[\left(\frac{N_L}{s\mathcal{G}(\phi_\mathbf{v},\omega)\,C_L\left(r_P^2+r_t^2-2r_Pr_t\cos\theta_t+\hat{h}^2\right)^{-\frac{\alpha_L}{2}}+N_L}\right)^{N_L}\right]\right] \\ &\overset{(c)}{=} \mathbb{E}_\mathcal{G}\left[\exp\left(-2\pi\lambda\sum_{\delta_{t_n}\in\mathbb{Z}^*}p_L(\delta_{t_n})\int_a^b\left(1-\left(1+\frac{\hat{s}(\phi_\mathbf{v},\omega,s)}{\left(r_P^2+\hat{h}^2\right)^{\frac{\alpha_L}{2}}}\right)^{-N_L}\right)r_P dr_P\right)\right]\end{aligned} \tag{A.3}$$

By substituting (A.5) and (A.6) into (A.1), we obtain (23).

In terms of the condition $\alpha_N \neq 2$ and $\alpha_L = 2$, the expression (A.6) for NLOS links keeps the same and (A.5) should be changed. Before calculating the exact expression for Θ_L, we introduce another integral as follows:

$$\begin{aligned} F_s(z) &= \int \left(\frac{1}{z^2(z+1)^{N_L}} - \frac{1}{z^2} \right) dz \\ &\overset{(f)}{=} N_L \ln\left(1+\frac{1}{z}\right) + \frac{(z+1)^{N_L-1}-1}{z(z+1)^{N_L-1}} \\ &\quad - \sum_{m=\min(1,N_L-1)}^{N_L-1} \frac{\mathbf{U}(N_L-2)N_L}{(z+1)^{N_L-m}(N_L-m)}, \end{aligned} \tag{A.7}$$

where (f) follows (2.117-1), (2.117-3) and (2.118-1) in [50]. Applying (A.7) into (A.3), we obtain

$$\begin{aligned} \Theta_L &= \mathbb{E}_{\mathcal{G}} \Bigg[\exp\Bigg(-2\pi\lambda \sum_{\delta_{t_n} \in \mathbb{Z}^*} p_L(\delta_{t_n}) \frac{\hat{s}(\phi_{\mathbf{v}}, \omega, s)}{2} \\ &\quad \times \left(F_s\left(\frac{\hat{s}(\phi_{\mathbf{v}}, \omega, s)}{b^2+\hat{h}^2} \right) - F_s\left(\frac{\hat{s}(\phi_{\mathbf{v}}, \omega, s)}{a^2+\hat{h}^2} \right) \right) \Bigg) \Bigg] \\ &\overset{(d)}{=} \exp\left(-2\lambda \sum_{\delta_{t_n} \in \mathbb{Z}^*} p_L(\delta_{t_n}) \int_0^1 \int_0^\pi \mathcal{G}_{I_2}^L(\phi_{\mathbf{v}}, \omega, s)\, d\phi_{\mathbf{v}} d\omega \right) \end{aligned} \tag{A.8}$$

By substituting (A.8) and (A.6) into (A.1), we obtain (26). The proof is complete.

Appendix B: Proof of Theorem 1

The typical user connects to the typical UAV with two types of transmission: LOS transmission $P_{RS}^L(\Upsilon_{th})$ and NLOS transmission $P_{RS}^N(\Upsilon_{th})$. By substituting (14) into (30), the coverage probability $P_{RS}(\Upsilon_{th})$ is given by

$$\begin{aligned} P_{RS}(\Upsilon_{th}) &= \mathbb{P}\left[\frac{\mathrm{L}(u)|h_{\mathbf{v}_0}|^2}{I+\sigma_n^2} > \Upsilon_{th}, u = \|\mathbf{p}_0\| \right] \\ &= P_{RS}^L(\Upsilon_{th}) + P_{RS}^N(\Upsilon_{th}). \end{aligned} \tag{B.1}$$

We first deriving the LOS transmission $P_{RS}^L(\Upsilon_{th})$ based on (18), which is shown at the bottom of this page. In (B.2), (a) follows the tight upper bound for the normalized gamma variable $|h|^2$, which is $\mathbb{P}\left[|h|^2 < \psi\right] < \left(1-e^{-\psi\eta_L}\right)^{N_L}$ [10], [22], [51]. (b) obeys the Binomial theorem and the definition of Laplace of interference. (c) follows the Gaussian-Chebyshev quadrature equation, where i_2 and n_2 are used for distinguishing those i_1 and n_1 in the Laplace transform of interference.

With the similar method, the NLOS transmission $P_{RS}^N(\Upsilon_{th})$ can be expressed as

$$\begin{aligned} &P_{RS}^N(\Upsilon_{th}) \\ &\approx \frac{\pi}{2n_2\sqrt{\lambda_a\lambda_b}} \sum_{i_2=1}^{n_2} \sqrt{1-\zeta_{i_2}^2} \sum_{\delta_u \in \mathbb{Z}^*} (1-p_L(\delta_u)) \\ &\quad \times \sum_{n_N=1}^{N_N} (-1)^{n_N+1} \binom{N_N}{n_N} \Psi_N\left(\frac{\zeta_{i_2}+2\delta_u+1}{2\sqrt{\lambda_a\lambda_b}} \right). \end{aligned} \tag{B.3}$$

Then by substituting (B.2) and (B.3) into (B.1), we obtain (31). The proof is complete.

Appendix C: Proof of Corollary 3

Under special case 2, the NLOS transmission and interference can be ignored. Based on (14), the exact the coverage probability can be expressed as

$$\begin{aligned} &\tilde{P}_{RS}^n(\Upsilon_{th}) \\ &= \mathbb{P}\left[\frac{\mathrm{L}(u)|h_{\mathbf{v}_0}|^2}{\sigma_n^2} < \Upsilon_{th}, u = \|\mathbf{p}_0\| \right] \\ &= \int_0^\infty p_L(\delta_u) \mathbb{P}\left[|h|^2 < \frac{\Upsilon_{th}\sigma_n^2}{C_L\left(u^2+\hat{h}^2\right)^{-\frac{\alpha_L}{2}}} \right] f_{RS}(u)\, du \\ &\overset{(a)}{=} \int_0^\infty p_L(\delta_u) \left(1 - \frac{\gamma\left(N_L, \frac{N_L\Upsilon_{th}\sigma_n^2}{C_L(u^2+\hat{h}^2)^{-\frac{\alpha_L}{2}}}\right)}{(N_L-1)!} \right) f_{RS}(u)\, du, \end{aligned} \tag{C.1}$$

where (a) follows the fact the CDF of normalized gamma variable $|h|^2$ with the parameter N_L is $\mathbb{P}[|h|^2 < x] = \frac{\gamma(N_L, N_L x)}{\Gamma(N_L)}$. Since N_L is a positive integer in this paper,

$$\begin{aligned} P_{RS}^L(\Upsilon_{th}) &= \int_0^\infty p_L(\delta_u) \mathbb{P}\left[|h|^2 > \frac{\Upsilon_{th}\left(I+\sigma_n^2\right)}{C_L\left(u^2+\hat{h}^2\right)^{-\frac{\alpha_L}{2}}}, u = \|\mathbf{p}_0\| \right] f_{RS}(u)\, du \\ &\overset{(a)}{\approx} \int_0^\infty p_L(\delta_u) \left(1 - \mathbb{E}\left[\left(1 - \exp\left(-\frac{\eta_L\Upsilon_{th}\left(I+\sigma_n^2\right)}{C_L\left(u^2+\hat{h}^2\right)^{-\frac{\alpha_L}{2}}} \right) \right)^{N_L} \right] \right) f_{RS}(u)\, du \\ &\overset{(b)}{=} \sum_{\delta_u \in \mathbb{Z}^*} p_L(\delta_u) \sum_{n_L=1}^{N_L} (-1)^{n_L+1} \binom{N_L}{n_L} \int_{\frac{\delta_u}{\sqrt{\lambda_a\lambda_b}}}^{\frac{\delta_u+1}{\sqrt{\lambda_a\lambda_b}}} \Psi_L(u)\, du, \quad \left(\delta_u = \left\lfloor u\sqrt{\lambda_a\lambda_b} \right\rfloor\right) \\ &\overset{(c)}{=} \frac{\pi}{2n_2\sqrt{\lambda_a\lambda_b}} \sum_{i_2=1}^{n_2} \sqrt{1-\zeta_{i_2}^2} \sum_{\delta_u \in \mathbb{Z}^*} p_L(\delta_u) \sum_{n_L=1}^{N_L} (-1)^{n_L+1} \binom{N_L}{n_L} \Psi_L\left(\frac{\zeta_{i_2}+2\delta_u+1}{2\sqrt{\lambda_a\lambda_b}} \right), \end{aligned} \tag{B.2}$$

the gamma function $\Gamma(N_L) = (N_L - 1)!$. Then by substituting (18) into (C.1), we obtain

$$\begin{aligned}
&\tilde{P}_{RS}^{n}\left(\Upsilon_{th}\right) \\
&= \sum_{\delta_u \in \mathbb{Z}^*} p_L\left(\delta_u\right) \\
&\quad \times \int_{\frac{\delta_u}{\sqrt{\lambda_a \lambda_b}}}^{\frac{\delta_u+1}{\sqrt{\lambda_a \lambda_b}}} \left(1 - \frac{\gamma\left(N_L, \frac{N_L \Upsilon_{th} \sigma_n^2}{C_L (u^2+\hat{h}^2)^{-\frac{\alpha_L}{2}}}\right)}{(N_L-1)!}\right) f_{RS}\left(u\right) du \\
&\overset{(b)}{=} \frac{\pi}{2n_2\sqrt{\lambda_a \lambda_b}} \\
&\quad \times \sum_{i_2=1}^{n_2} \sqrt{1-\zeta_{i_2}^2} \sum_{\delta_u \in \mathbb{Z}^*} p_L\left(\delta_u\right) \Psi_L^n \left(\frac{\zeta_{i_2}+2\delta_u+1}{2\sqrt{\lambda_a \lambda_b}}\right), \quad \text{(C.2)}
\end{aligned}$$

where (b) uses the Gaussian-Chebyshev quadrature equation with $a = \delta_u/\sqrt{\lambda_a \lambda_b}$, $b = (\delta_u + 1)/\sqrt{\lambda_a \lambda_b}$. The proof is complete.

REFERENCES

[1] W. Yi, Y. Liu, M. Elkashlan, and A. Nallanathan, "Modeling and coverage analysis of downlink UAV networks with MmWave communications," in *Proc. IEEE Int. Conf. Commun. Workshops (ICC Workshops)*, May 2019, pp. 1–6.

[2] Y. Zeng, R. Zhang, and T. J. Lim, "Wireless communications with unmanned aerial vehicles: Opportunities and challenges," *IEEE Commun. Mag.*, vol. 54, no. 5, pp. 36–42, May 2016.

[3] A. Merwaday and I. Guvenc, "UAV assisted heterogeneous networks for public safety communications," in *Proc. IEEE Wireless Commun. Netw. Conf. Workshops (WCNCW)*, Mar. 2015, pp. 329–334.

[4] T. Hou, Y. Liu, Z. Song, X. Sun, and Y. Chen, "Exploiting NOMA for UAV communications in large-scale cellular networks," *IEEE Trans. Commun.*, vol. 67, no. 10, pp. 6897–6911, Oct. 2019.

[5] Z. Xiao, P. Xia, and X.-G. Xia, "Enabling UAV cellular with millimeter-wave communication: Potentials and approaches," *IEEE Commun. Mag.*, vol. 54, no. 5, pp. 66–73, May 2016.

[6] Y. Zeng, X. Xu, and R. Zhang, "Trajectory design for completion time minimization in UAV-enabled multicasting," *IEEE Trans. Wireless Commun.*, vol. 17, no. 4, pp. 2233–2246, Apr. 2018.

[7] Y. Zeng and R. Zhang, "Energy-efficient UAV communication with trajectory optimization," *IEEE Trans. Wireless Commun.*, vol. 16, no. 6, pp. 3747–3760, Jun. 2017.

[8] M. Chen, M. Mozaffari, W. Saad, C. Yin, M. Debbah, and C. S. Hong, "Caching in the sky: Proactive deployment of cache-enabled unmanned aerial vehicles for optimized quality-of-experience," *IEEE J. Sel. Areas Commun.*, vol. 35, no. 5, pp. 1046–1061, May 2017.

[9] M. Chen, W. Saad, and C. Yin, "Liquid state machine learning for resource and cache management in LTE-U unmanned aerial vehicle (UAV) networks," *IEEE Trans. Wireless Commun.*, vol. 18, no. 3, pp. 1504–1517, Mar. 2019.

[10] T. Bai and R. W. Heath, Jr., "Coverage and rate analysis for millimeter-wave cellular networks," *IEEE Trans. Wireless Commun.*, vol. 14, no. 2, pp. 1100–1114, Feb. 2015.

[11] T. S. Rappaport, R. W. Heath, Jr., R. C. Daniels, and J. N. Murdock, *Millimeter Wave Wireless Communications*. London, U.K.: Pearson, 2014.

[12] T. S. Rappaport, F. Gutierrez, E. Ben-Dor, J. N. Murdock, Y. Qiao, and J. I. Tamir, "Broadband millimeter-wave propagation measurements and models using adaptive-beam antennas for outdoor urban cellular communications," *IEEE Trans. Antennas Propag.*, vol. 61, no. 4, pp. 1850–1859, Apr. 2013.

[13] Z. Pi and F. Khan, "An introduction to millimeter-wave mobile broadband systems," *IEEE Commun. Mag.*, vol. 49, no. 6, pp. 101–107, Jun. 2011.

[14] M. R. Akdeniz *et al.*, "Millimeter wave channel modeling and cellular capacity evaluation," *IEEE J. Sel. Areas Commun.*, vol. 32, no. 6, pp. 1164–1179, Jun. 2014.

[15] A. V. Alejos, M. G. Sanchez, and I. Cuinas, "Measurement and analysis of propagation mechanisms at 40 GHz: Viability of site shielding forced by obstacles," *IEEE Trans. Veh. Technol.*, vol. 57, no. 6, pp. 3369–3380, Nov. 2008.

[16] D. Maamari, N. Devroye, and D. Tuninetti, "Coverage in mmWave cellular networks with base station co-operation," *IEEE Trans. Wireless Commun.*, vol. 15, no. 4, pp. 2981–2994, Apr. 2016.

[17] *Propagation Data and Prediction Methods Required for the Design of Terrestrial Broadband Radio Access Systems Operating in a Frequency Range From 3 to 60 GHz*, document TR-REC-P.1410, ITU-R, 2012.

[18] W. Roh *et al.*, "Millimeter-wave beamforming as an enabling technology for 5G cellular communications: Theoretical feasibility and prototype results," *IEEE Commun. Mag.*, vol. 52, no. 2, pp. 106–113, Feb. 2014.

[19] S. Rangan, T. S. Rappaport, and E. Erkip, "Millimeter-wave cellular wireless networks: Potentials and challenges," *Proc. IEEE*, vol. 102, no. 3, pp. 366–385, Mar. 2014.

[20] J. G. Andrews *et al.*, "What will 5G be?" *IEEE J. Sel. Areas Commun.*, vol. 32, no. 6, pp. 1065–1082, Jun. 2014.

[21] F. Boccardi, R. W. Heath, Jr., A. Lozano, T. L. Marzetta, and P. Popovski, "Five disruptive technology directions for 5G," *IEEE Commun. Mag.*, vol. 52, no. 2, pp. 74–80, Feb. 2014.

[22] W. Yi, Y. Liu, and A. Nallanathan, "Modeling and analysis of D2D millimeter-wave networks with Poisson cluster processes," *IEEE Trans. Commun.*, vol. 65, no. 12, pp. 5574–5588, Dec. 2017.

[23] Y. Zhu, G. Zheng, and M. Fitch, "Secrecy rate analysis of UAV-enabled mmWave networks using Matérn hardcore point processes," *IEEE J. Sel. Areas Commun.*, vol. 36, no. 7, pp. 1397–1409, Jul. 2018.

[24] Y. Liu, Z. Ding, M. Elkashlan, and H. V. Poor, "Cooperative non-orthogonal multiple access with simultaneous wireless information and power transfer," *IEEE J. Sel. Areas Commun.*, vol. 34, no. 4, pp. 938–953, Apr. 2016.

[25] Y. Liu, Z. Qin, M. Elkashlan, A. Nallanathan, and J. A. McCann, "Non-orthogonal multiple access in large-scale heterogeneous networks," *IEEE J. Sel. Areas Commun.*, vol. 35, no. 12, pp. 2667–2680, Dec. 2017.

[26] V. V. Chetlur and H. S. Dhillon, "Downlink coverage analysis for a finite 3D wireless network of unmanned aerial vehicles," *IEEE Trans. Commun.*, vol. 65, no. 10, pp. 4543–4558, Oct. 2017.

[27] T. Hou, Y. Liu, Z. Song, X. Sun, and Y. Chen, "Multiple antenna aided NOMA in UAV networks: A stochastic geometry approach," *IEEE Trans. Commun.*, vol. 67, no. 2, pp. 1031–1044, Feb. 2019.

[28] B. Galkin, J. Kibiłda, and L. A. DaSilva, "A stochastic geometry model of backhaul and user coverage in urban UAV networks," 2017, *arXiv:1710.03701*. [Online]. Available: http://arxiv.org/abs/1710.03701

[29] J. Ye, C. Zhang, H. Lei, G. Pan, and Z. Ding, "Secure UAV-to-UAV systems with spatially random UAVs," *IEEE Wireless Commun. Lett.*, vol. 8, no. 2, pp. 564–567, Apr. 2019.

[30] X. Yu, J. Zhang, M. Haenggi, and K. B. Letaief, "Coverage analysis for millimeter wave networks: The impact of directional antenna arrays," *IEEE J. Sel. Areas Commun.*, vol. 35, no. 7, pp. 1498–1512, Jul. 2017.

[31] S. Akoum, O. El Ayach, and R. W. Heath, Jr., "Coverage and capacity in mmWave cellular systems," in *Proc. 46th Conf. Rec. Asilomar Conf. Signals, Syst. Comput. (ASILOMAR)*, Nov. 2012, pp. 688–692.

[32] W. Yi, Y. Liu, E. Bodanese, A. Nallanathan, and G. K. Karagiannidis, "A unified spatial framework for UAV-aided mmWave networks," *IEEE Trans. Commun.*, vol. 67, no. 12, pp. 8801–8817, Dec. 2019.

[33] M. Afshang, H. Dhillon, and P. Chong, "Modeling and performance analysis of clustered device-to-device networks," *IEEE Trans. Wireless Commun.*, vol. 15, no. 7, pp. 4957–4972, Jul. 2016.

[34] M. Samimi *et al.*, "28 GHz angle of arrival and angle of departure analysis for outdoor cellular communications using steerable beam antennas in New York city," in *Proc. IEEE 77th Veh. Technol. Conf. (VTC Spring)*, Jun. 2013, pp. 1–6.

[35] G. D. Durgin and T. S. Rappaport, "Theory of multipath shape factors for small-scale fading wireless channels," *IEEE Trans. Antennas Propag.*, vol. 48, no. 5, pp. 682–693, May 2000.

[36] T. S. Rappaport, G. R. MacCartney, M. K. Samimi, and S. Sun, "Wideband millimeter-wave propagation measurements and channel models for future wireless communication system design," *IEEE Trans. Commun.*, vol. 63, no. 9, pp. 3029–3056, Sep. 2015.

[37] Y. Tsai, L. Zheng, and X. Wang, "Millimeter-wave beamformed full-dimensional MIMO channel estimation based on atomic norm minimization," *IEEE Trans. Commun.*, vol. 66, no. 12, pp. 6150–6163, Dec. 2018.

[38] D. Fan, F. Gao, G. Wang, Z. Zhong, and A. Nallanathan, "Angle domain signal processing-aided channel estimation for indoor 60-GHz TDD/FDD massive MIMO systems," *IEEE J. Sel. Areas Commun.*, vol. 35, no. 9, pp. 1948–1961, Sep. 2017.

[39] R. W. Heath, Jr., N. Gonzalez-Prelcic, S. Rangan, W. Roh, and A. M. Sayeed, "An overview of signal processing techniques for millimeter wave MIMO systems," *IEEE J. Sel. Topics Signal Process.*, vol. 10, no. 3, pp. 436–453, Apr. 2016.

[40] W. Yi, Y. Liu, A. Nallanathan, and M. Elkashlan, "Clustered millimeter-wave networks with non-orthogonal multiple access," *IEEE Trans. Commun.*, vol. 67, no. 6, pp. 4350–4364, Jun. 2019.
[41] D. Stoyan, W. Kendall, and J. Mecke, *Stochastic Geometry and Its Applications*. Berlin, Germany: Akademie-Verlag, 1995.
[42] H. A. David and H. N. Nagaraja, "Order statistics," in *Encyclopedia of Statistical Sciences*, 3rd ed. Hoboken, NJ, USA: Wiley, 2003.
[43] A. Thornburg, T. Bai, and R. W. Heath, Jr., "Performance analysis of outdoor mmWave ad hoc networks," *IEEE Trans. Signal Process.*, vol. 64, no. 15, pp. 4065–4079, Aug. 2016.
[44] H. Elshaer, M. N. Kulkarni, F. Boccardi, J. G. Andrews, and M. Dohler, "Downlink and uplink cell association with traditional macrocells and millimeter wave small cells," *IEEE Trans. Wireless Commun.*, vol. 15, no. 9, pp. 6244–6258, Sep. 2016.
[45] Y. Azar *et al.*, "28 GHz propagation measurements for outdoor cellular communications using steerable beam antennas in New York city," in *Proc. IEEE Int. Conf. Commun. (ICC)*, Jun. 2013, pp. 5143–5147.
[46] T. S. Rappaport, E. Ben-Dor, J. N. Murdock, and Y. Qiao, "38 GHz and 60 GHz angle-dependent propagation for cellular & peer-to-peer wireless communications," in *Proc. IEEE Proc. Int. Commun. Conf. (ICC)*, Jun. 2012, pp. 4568–4573.
[47] C. A. Balanis, *Antenna Theory: Analysis and Design*. Hoboken, NJ, USA: Wiley, 2016.
[48] Z. Ding, P. Fan, and H. V. Poor, "Random beamforming in millimeter-wave NOMA networks," *IEEE Access*, vol. 5, pp. 7667–7681, 2017.
[49] W. Yi, Y. Liu, and A. Nallanathan, "Cache-enabled HetNets with millimeter wave small cells," *IEEE Trans. Commun.*, vol. 66, no. 11, pp. 5497–5511, Nov. 2018.
[50] A. Jeffrey and D. Zwillinger, *Table of Integrals, Series, and Products*. New York, NY, USA: Academic, 2007.
[51] H. Alzer, "On some inequalities for the incomplete gamma function," *Math. Comput.*, vol. 66, no. 218, pp. 771–779, Apr. 1997.

Wenqiang Yi (Student Member, IEEE) received the B.S. degree in optical information science and technology from the Wuhan University of Technology, China, in 2012, and the M.S. degree in wireless communications and signal processing from the University of Bristol, U.K., in 2013. He completed his first year of doctoral study with the Centre for Telecommunications Research, Department of Informatics, King's College London, in September 2016. He is currently pursuing the Ph.D. degree with the Communication Systems Research Group, School of Electronic Engineering and Computer Science, Queen Mary University of London.

His research interests include mmWave networks, NOMA, UAV/V2X communications, stochastic geometry, and deep reinforcement learning. He received the Exemplary Reviewer Award of IEEE TRANSACTIONS ON COMMUNICATIONS in 2019.

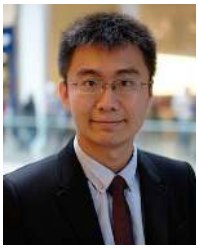

Yuanwei Liu (Senior Member, IEEE) received the B.S. and M.S. degrees from the Beijing University of Posts and Telecommunications in 2011 and 2014, respectively, and the Ph.D. degree in electrical engineering from the Queen Mary University of London, U.K., in 2016.

He was with the Department of Informatics, King's College London, from 2016 to 2017, where he was a Post-Doctoral Research Fellow. He has been a Lecturer (Assistant Professor) with the School of Electronic Engineering and Computer Science, Queen Mary University of London, since 2017. His research interests include 5G wireless networks, Internet of Things, machine learning, stochastic geometry, and matching theory. He received the Exemplary Reviewer Certificate of IEEE WIRELESS COMMUNICATION LETTERS in 2015 and IEEE TRANSACTIONS ON COMMUNICATIONS and IEEE TRANSACTIONS ON WIRELESS COMMUNICATIONS in 2016 and 2017, respectively. He has served as a TPC member for many IEEE conferences, such as GLOBECOM and ICC. He currently serves as an Editor for IEEE TRANSACTIONS ON COMMUNICATIONS, IEEE COMMUNICATIONS LETTERS, and IEEE ACCESS. He is also a Guest Editor for IEEE JOURNAL OF SELECTED TOPICS IN SIGNAL PROCESSING (JSTSP) special issue on Signal Processing Advances for Non-Orthogonal Multiple Access in Next Generation Wireless Networks.

Yansha Deng (Member, IEEE) received the Ph.D. degree in electrical engineering from the Queen Mary University of London, U.K., in 2015. From 2015 to 2017, she was a Post-Doctoral Research Fellow at King's College London, U.K., where she is currently a Lecturer (Assistant Professor) with the Department of Informatics. Her research interests include molecular communication, machine learning, and 5G wireless networks. She was a recipient of the Best Paper Awards from ICC 2016 and Globecom 2017 as the first author. She is currently an Associate Editor of IEEE TRANSACTIONS ON COMMUNICATIONS, IEEE TRANSACTIONS ON MOLECULAR, BIOLOGICAL AND MULTI-SCALE COMMUNICATIONS, and the Senior Editor of IEEE COMMUNICATION LETTERS. She also received the Exemplary Reviewers of IEEE TRANSACTIONS ON COMMUNICATIONS in 2016 and 2017, and IEEE TRANSACTIONS ON WIRELESS COMMUNICATIONS in 2018. She has also served as a TPC member for many IEEE conferences, such as IEEE GLOBECOM and ICC.

Arumugam Nallanathan (Fellow, IEEE) was with the Department of Informatics, King's College London, from December 2007 to August 2017, where he was a Professor of wireless communications from April 2013 to August 2017, and has been a Visiting Professor since September 2017. He was an Assistant Professor at the Department of Electrical and Computer Engineering, National University of Singapore, from August 2000 to December 2007. He is currently a Professor of wireless communications, and has been the Head of the Communication Systems Research (CSR) Group, School of Electronic Engineering and Computer Science, Queen Mary University of London, since September 2017. He has published nearly 500 technical papers in scientific journals and international conferences. His research interests include artificial intelligence for wireless systems, beyond 5G wireless networks, Internet of Things (IoT), and molecular communications.

Dr. Nallanathan received the IEEE Communications Society SPCE Outstanding Service Award 2012 and IEEE Communications Society RCC Outstanding Service Award 2014. He has served as the Chair for the Signal Processing and Communication Electronics Technical Committee of IEEE Communications Society and Technical Program Chair and a member of Technical Program Committees in numerous IEEE conferences. He is a co-recipient of the Best Paper Awards presented at the IEEE International Conference on Communications 2016 (ICC'2016), IEEE Global Communications Conference 2017 (GLOBECOM'2017), and IEEE Vehicular Technology Conference 2018 (VTC'2018). He is an IEEE Distinguished Lecturer. He has been selected as a Web of Science Highly Cited Researcher in 2016. He is an Editor of IEEE TRANSACTIONS ON COMMUNICATIONS. He was an Editor of IEEE TRANSACTIONS ON WIRELESS COMMUNICATIONS (2006–2011), IEEE TRANSACTIONS ON VEHICULAR TECHNOLOGY (2006–2017), IEEE WIRELESS COMMUNICATIONS LETTERS, and IEEE SIGNAL PROCESSING LETTERS.